JCTC Journal of Chemical Theory and Computation

Implementation and Performance of DFT-D with Respect to Basis Set and Functional for Study of Dispersion Interactions in Nanoscale Aromatic Hydrocarbons

Roberto Peverati and Kim K Baldridge*

University of Zürich, Winterthurerstrasse 190, CH-8057 Zürich

Received June 27, 2008

Abstract: The implementation, optimization, and performance of various DFT-D schemes have been tested on models for polar$-\pi$ interactions between arenes spaced at van der Waals distances and on a series of functionalized corannulene derivatives and complexes. For DFT-D schemes involving a semiempirical correction, optimized parameters are proposed for several basis sets. Performance of the different DFT-D strategies is compared, where functionals include some of the most recently proposed, B97D, B2PLYP, BMK, and M06−2X functionals, together with several other well-known functionals. Semiempircally corrected dispersion functionals hold some promise as useful and affordable methods for studies involving large polynuclear aromatic molecules and molecules on metal surfaces.

Introduction

Aromatic carbon nanosystems display subtle dependencies among their structure, dynamics, and photophysical properties that make them challenging to model computationally. The challenges lie in the treatment of electron correlation, dispersion, polarization, and solvation, in a manner appropriate to the context of the application and within the limits of available computational resources. Investigations of polynuclear aromatic hydrocarbons have revealed weaknesses in commonly used computational theories regarding the treatment of delocalization and dispersion effects.[1−10] Delocalization lies at the heart of the concept of aromaticity, and the importance of van der Waals (vdW) interactions comes from the large surface areas of interaction and polarizable electron densities. Dispersion energies are a pure electron correlation effect,[11,12] whereas delocalization involves both short- and long-range effects. Accurate computations via higher-order *ab initio* based wave functions, such as CCSD(T), reach a good level of accuracy with large basis sets[13] but are prohibitively costly for even relatively small systems. Cheaper methods, such as Møller−Plesset perturbation (MP2),[14] still become costly when over 1000 basis functions are considered. In addition, they tend to overestimate the electron correlation contribution,[15,16] for example, that stemming from pure $\pi-\pi$ interactions.[17,18]

Density functional theory (DFT) offers the hope of tackling large systems in a broad context with reasonable effort and appears to be less basis set dependent than can be the more advanced wave function methods.[19,20] However, treatment of noncovalent interactions must be addressed on a functional and basis set level, significantly complicating general applicability. Conventional DFT techniques fail to treat dispersion effects completely. Recently, the DFT community has developed a variety of methods for the treatment of van der Waals (dispersion) interactions, including treatments with specialized functionals, such as BMK[21] and the M05[22]/M06[23] series, semiempirically dispersion corrected functionals, such as B97D,[24] and double hybrid functionals, such as B2PLYP.[25] The hierarchy of methods.[24−51] parallels the sophistication of the treatment of the exchange-correlation potential, $E_{xc} = aE_x + bE_{HF} + cE_c$, where the exchange and correlation terms each may be a mixture of terms with different weights. Proper balance of exchange, accounting for antisymmetry caused by the Pauli exclusion principle, and correlation accounting for many-bodied effects are necessary to adequately describe the delocalization phenomenon in these aromatic carbon systems. The sheer size of systems involving corannulene-based molecular recognition chemistry would be prohibitively expensive using conven-

* To whom correspondence should be addressed. Tel: +41 44 635 4201. Fax: +41 44 635 6888. E-mail: kimb@oci.uzh.ch.

10.1021/ct800252z CCC: $40.75
Published on Web 10/28/2008

tional wave function strategies, and therefore, DFT tends to be the most practical choice. As such, aromatic carbon nanosystems provide a good 'test bed' for implementation and optimization of DFT-based dispersion (DFT-D) models. Our goals in this work include, (a) contribution to the development of semiempirically corrected density functionals, emphasizing functionals and basis sets that are necessary for polynuclear aromatic carbon nanosystems, (b) implementation of several dispersion corrected functionals (via both semiempirical corrections as well as double-hybrid functionals) into our computational chemistry software, GAMESS,[52] and (c) development of a hybrid model for extended materials and corannulene-functionalized metallic surfaces, using GAMESS together with the materials software, SIESTA,[53] the latter of which is more limited in basis set and density functional representation.

Computational Methods

All calculations reported here were carried out using a locally modified version of the GAMESS electronic structure program,[52] and the SIESTA electronic simulations software,[54,55] running on the Baldridge group Linux cluster at UZH, and the latter also running CSCS supercomputer. Here, we consider several classes of DFT functionals including, M06−2X,[23] BMK,[21] several empirically corrected conventional functionals, PBE,[47] revPBE,[56] BP86,[57−59] B3LYP,[60,61] B97D,[24] and the double-hybrid functional B2PLYP.[25] In addition, some comparisons are made with the second-order Møller−Plesset perturbation theory (MP2). [14] In the case of the semiempircally corrected functionals, given the importance and dependence of the associated parameters on the choice of functional and basis set, we have carried out parameter optimization for several basis sets, including TZV2P,[62] with (2d,2p), and Dunning's correlation consistent basis sets,[63] denoted cc-pVnZ, where n = D for double with [3s2p1d] contraction, T for triple with [4s3p2d1f] contraction, and Q for quadruple with [5s4p3d2f1g] contraction. Finally, we have constructed a double-ζ quality (3d,4s,4p) basis set supplemented with extra diffuse (5s) functions for the corannulene on Cu(111) surface computations, as per the localized atomic orbital basis set specifications in SIESTA. The quality of the basis set was checked against surface energy, work function, and interlayer relaxation for the clean Cu(111) surface. The S22 reference set of data provided by Jurecka et al. [64] has been used as a validation test set, in addition to several other small dimers.

Theoretical Approach and Discussion

Empirical Correction. Perhaps motivated by the possibility of a more simplistic approach, several methods for correcting DFT for failures involving noncovalent interactions have involved addition of an empirical correction to the final DFT energy,[42,65] typically of the form C_6R^{-6}, where R represents the interatomic distances and C_6 the dispersion coefficients. Such a strategy has been formulated and well established by several research groups. [24,39,40,66]

We have also implemented such a formulation into our computational software, GAMESS,[52] as well as in the SIESTA software in our collaborative effort, as

$$E_{\mathrm{disp}} = -s_6 \sum_{i=1}^{N_{\mathrm{nat}}-1} \sum_{j=i+1}^{N_{\mathrm{nat}}} \frac{C_6^{ij}}{R_{ij}^6} f_{\mathrm{dmp}}(R_{ij}) \quad (1)$$

with

$$f_{\mathrm{dmp}} = 1/(1+\exp(-d(r_{ij}/s_R R_{ij}^0)-1)) \quad (2)$$

This scheme is general and can be applied not only to DFT but also to all mean field methods that lack a sufficient treatment of dispersion energy.[67,68] The main parameters in this scheme are (a) the C_6^{ij} coefficients, (b) the R_0 vdW radii, and (c) all of the scale factors. Differences in implementations are mainly in the values of these parameters. For example, R_0 is typically calculated with wave function based methods and scaled by an appropriate factor; C_6 has been calculated from atomic hybridization states and also determined from LDF calculated IPs and static dipole polarizabilities, α, and the damping factor, d, typically takes on values between 20−23. C_6^{ij} can be determined via formulas such as $C_6^{ij} = \sqrt{(C_6^i C_6^j)}$, which has been found by Grimme to be consistent for problems of interest in this work, and the functional dependent scale factors, s_6, typically determined via parameter fitting. The final mean-field (MF) DFT-D energy is the result of the direct addition of this dispersion energy to the computed DFT energy:

$$E_{\mathrm{MF\text{-}D}} = E_{\mathrm{MF}} + E_{\mathrm{disp}} \quad (3)$$

Employing this strategy, three parameters are of concern: the s_6 prefactor to the C_6 atomic coefficients, the d damping factor, and the s_R prefactor to the vdW radii. The nonlinear parameter, d, is considered optimal and is fixed to the optimized value of Grimme, $d = 20$.[24]

In this work, we consider dependencies of both s_6 and s_R parameters simultaneously, with respect to basis sets and common functionals. Parameters for the several functionals are proposed for the first time, including those for the revised-PBE (revPBE) functional,[47,69] which has particular importance for our extensions of GAMESS with SIESTA[53] for computations involving materials.

Double Parameter Optimization. There has been substantial discussion in the recent DFT-D literature concerning the issue of the optimization of the parameters for the semiempircal correction (eq 1).[39,42,70] Many consider a fixed value of s_R and optimize the linear parameter s_6 (as in the original work of Grimme).[24,40] The atomic dispersion coefficient prefactors s_6 were originally optimized by Grimme using the TZV2P (also referred as TZV(2d,2p)) basis set, suggesting a fixed value of $s_R = 1.1$. Optimization of the nonlinear vdW factor s_R, keeping s_6 at one (as in the work of Jurecka), has also been considered,[39] because it has a more complete optimization of all empirical parameters of a damping function for C_6R^{-6} for three specific functionals (PBE, BP86, B3LYP) and several basis sets for application to π-stacking interactions in nucleic acids.[71] Given the importance of these parameters on the ultimate predictability of DFT-D, as well as the need to add the appropriate dispersion correction term for the specific functional and basis set being used, we have considered a simultaneous double optimization of the two parameters, showing the behavior of both parameters across various functionals and

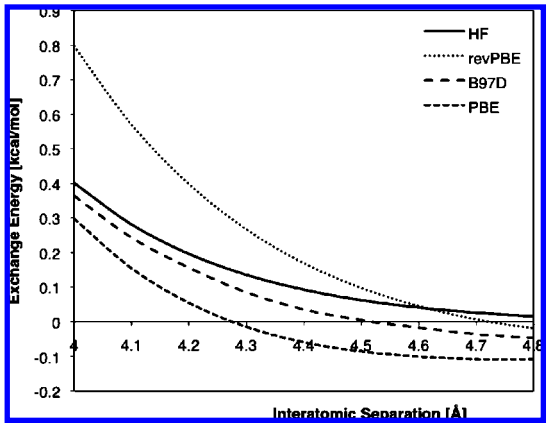

Figure 1. Plot of the exchange energy of the functionals, PBE, revPBE, and B97D, compared to the exact Hartree−Fock exchange in the vdW region, for the Kr_2 dimer.

basis sets. We propose optimal values of both parameters for each case.

The S22 reference set of data provided by Jurecka et al.[64] has been used for determination of the optimized parameters, a common choice for studies of the present type. As in previous works, [24,64] the two parameters were optimized by variation of their values so that the difference between reference single point energy and the DFT-D for the same geometry is minimized. Accurate geometries were taken for the S22 set from the original paper. All DFT-D calculations were performed with the newly modified GAMESS software.

For consideration of double optimization, we have implemented and tested the recently developed B97D exchange-correlation functional,[24] into GAMESS. This functional is a special reparametrization of the original Becke 1997 functional together with a semiempircal correction. Grimme paid particular attention to avoid a so-called "double-counting" especially in large molecules, where many electron correlations at intermediate distances are accounted for both by the correction term and the functional itself. In the B97D functional, power expansion series coefficients of the original functional description were optimized by Grimme to restrict the density functional description to the shorter electron correlation ranges, while the medium to long-range descriptions are handled by the semiempirical correction term. In this case, $a = 1$ (function of 3 parameters), $b = 0$, and $c = 1$ (function of 6 parameters), using the notation presented in the introduction, $E_{xc} = aE_x + bE_{HF} + cE_c$.

B97D tends to be, in fact, much more insensitive to spurious contamination caused by parametrizations in the exchange component, that in some functionals mimics the dispersion effects. This effect can be more clearly observed by plotting the exchange energy of the functionals together with the exact Hartree−Fock exchange in the vdW region for a simple dimer of noble gas atoms, for example Kr, as shown in Figure 1.

The Zhang and Yang functional, revPBE,[56] employs a parametric fit to exact exchange data, and therefore is another candidate for addition of semiempirical dispersion effects. In some cases, revPBE mimics the HF result, however tends to result in more expanded intramolecular geometries and loosely held complexes. While this is partially compensated for by the addition of the attractive dispersion term, the overall effect is still lacking. In addition, one observes a rather large value for s_6 for revPBE because the correction is taking into account some effects that are typically handled with a correlation terms, which are not present in this functional.

Optimization of the empirical dispersion function parameter across the Dunning cc-pVnZ family of basis sets with $n = 2,3$, and the TZV(2d,2p) basis set used by Grimme in his original paper, was carried out for the B97D functional. Results are shown in Figure 2, where the median absolute deviation (MAD) is reported as a surface function of the two parameters s_R and s_6 for the S22 system of complexes.

In these diagrams, the lowest energy is given in red; the highest energy is in blue, and all plots are on the same relative scale. All plots in Figure 2 show a large region of red corresponding to optimal s_6 and s_R parameters where the MAD associated with the S22 set of complexes is at a minimum. For the cc-pVDZ basis set, the minimum functional region is 1.0 kcal/mol deep, while for both of the triple-ζ basis sets, the minimum functional region is 0.5 kcal/mol. One can find the intersection point between horizontal (s_6) and vertical (s_R) within this minimum region, as shown in the right most picture of each set of plots in Figure 2. A value of $s_R = 1.1$ always intercepts the minimum-regions, showing that optimization of s_R is not necessarily required, if combined with a good optimized value of the linear s_6 parameter. The intersection with an optimized value of s_6 (solid lines in the associated plots) always lies in the minimum-region. The values of s_6, as optimized by Grimme for TZV(2d,2p), are indicated as dashed lines for the first two sets of plots, to indicate the resulting difference when considering other basis sets.

A similar analysis was performed for the revPBE functional. Our particular interest in this functional is its suitability for our hybrid computations of corannulene on surfaces, using the SIESTA software. The revPBE is a good choice for such computations because it is found to be superior in the description of energetics of atomic and molecular bonding to surfaces, as compared to experimental findings. However, up to this point, the attractive dispersion term for this functional was lacking in both SIESTA and GAMESS.

Optimization results for the revPBE functional for one basis set is shown in Figure 3, with very similar characteristics for higher-order basis sets. As expected, the optimized s_6 value is quite large, at 1.66, because the correction is taking into account some effects that are typically handled with correlation terms, which are not present in this functional.

Double Hybrid Functional. In contrast to the strategy of including the effects of dispersion via an empirical function as discussed so far, an alternative strategy proposed in the literature for improving density functional theory even beyond the so-called fourth rung functionals, is via the "double-hybrid" functionals. [72] These functionals, as initially proposed, [73,74] involve a multilevel approach including more advanced *ab initio* components, within the density functional formalism, for example, Møller−Plesset theory. Double-hybrid functionals were then realized by Grimme in his

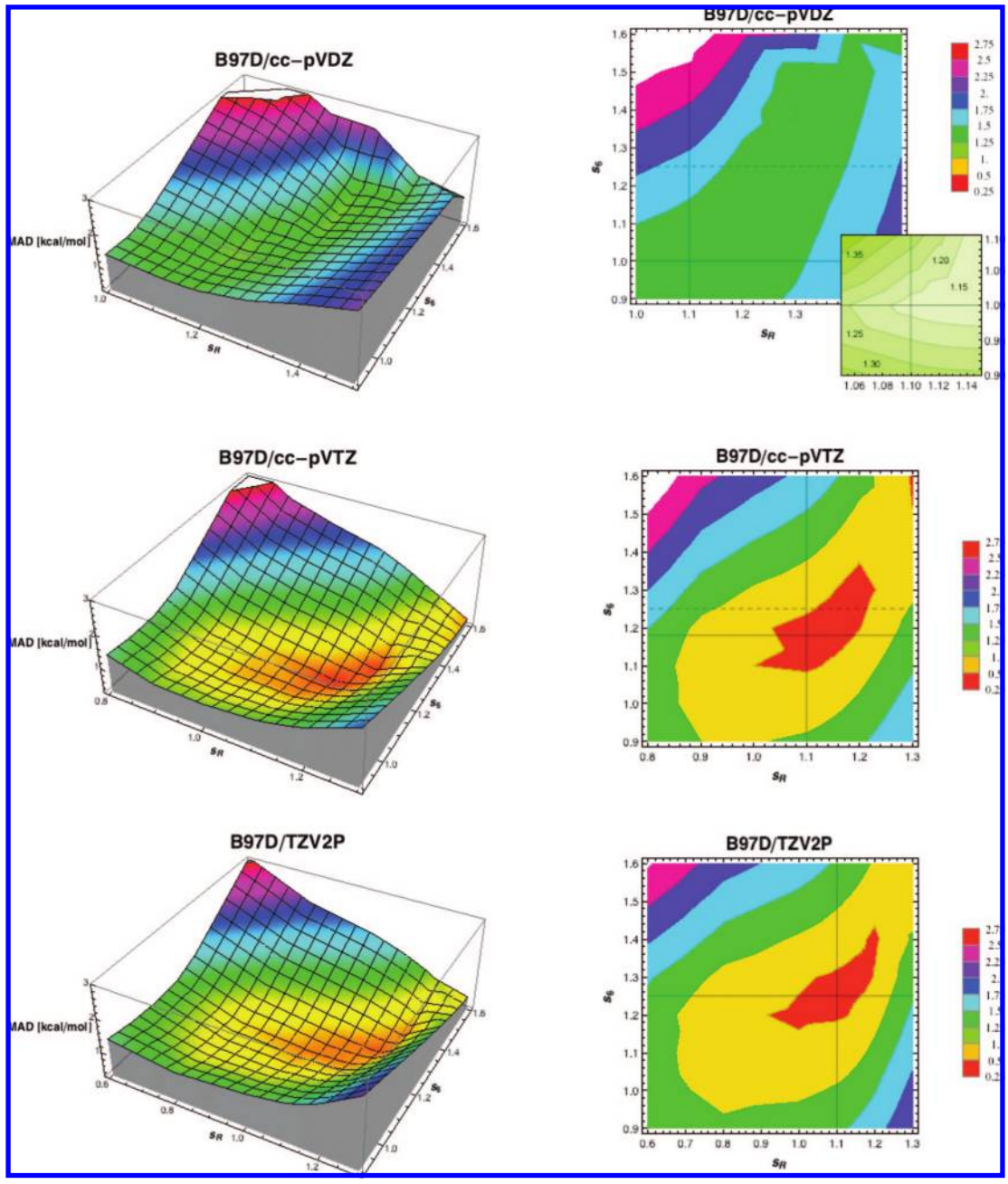

Figure 2. Optimized s_6 and s_R empirical dispersion function parameters for the B97D functional, with the cc-pVDZ, cc-pVTZ, and TZV(2d,2p) basis sets, respectively. All plots are given on the same relative scale, and a more detailed view of the minimum region is provided in the case of cc-pVDZ.

proposed B2PLYP set of functionals,[25,32] and later by others. In this type of treatment, typically either a hybrid density functional or meta-GGA functional is used together with exact HF exchange, but with a damped correlation functional. The remaining correlation is then treated with a more advanced *ab initio* method. In the case of B2PLYP, the meta-GGA functionals are LYP correlation[61] and B88 exchange,[57] with 53% exact HF exchange and 27% MP2 energy.

We have now implemented the B2PLYP functional into GAMESS, and considered optimal s_6 and s_R values for both the cc-pVDZ and cc-pVTZ basis sets. The resulting correlation plots are shown in Figure 4.

We observed results that are quite different from that found for the GGA and hybrid functionals. The s_6 parameter for the B2PLYP functional has a smaller optimized value (0.55), in part because of the dispersion contribution being taken into account with the PT2 component of the functional. However, the values are higher than zero because the PT2 component is scaled and takes into account only 27% of the dispersion. The s_R parameter will have a higher value for similar reasons. The differences found between the double-ζ and triple-ζ basis sets appear to be smaller than in the other functionals considered. In fact, the same pair of optimized s_6/s_R values can be utilized with good accuracy with either basis set. Therefore, we suggest values of $s_6 = 0.55$ and $s_R = 1.3$, which represent the best compromise between accuracy and general applicability. Again, the optimized values are

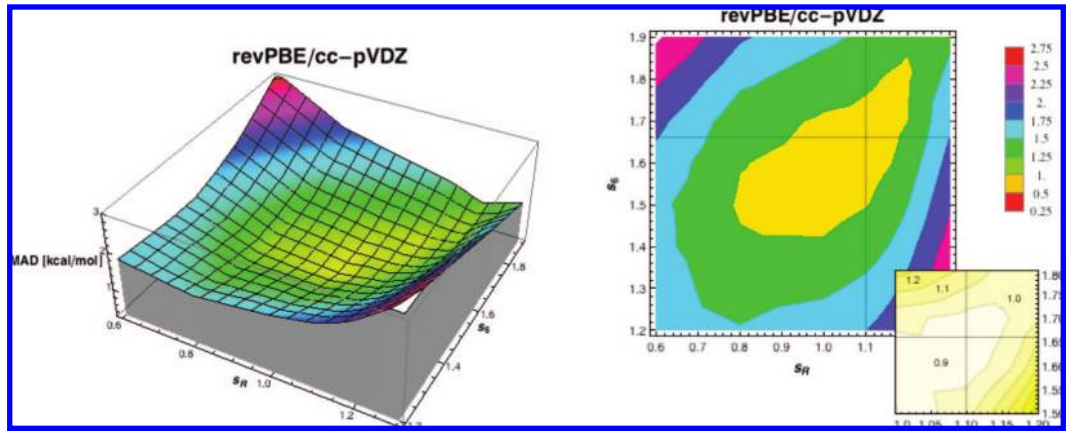

Figure 3. Optimized s_6 and s_R empirical dispersion function parameters for the revPBE functional, with the cc-pVDZ basis set. Plots are shown using the same relative scale as in Figure 2, and an inset showing a more detailed view of the minimum is provided.

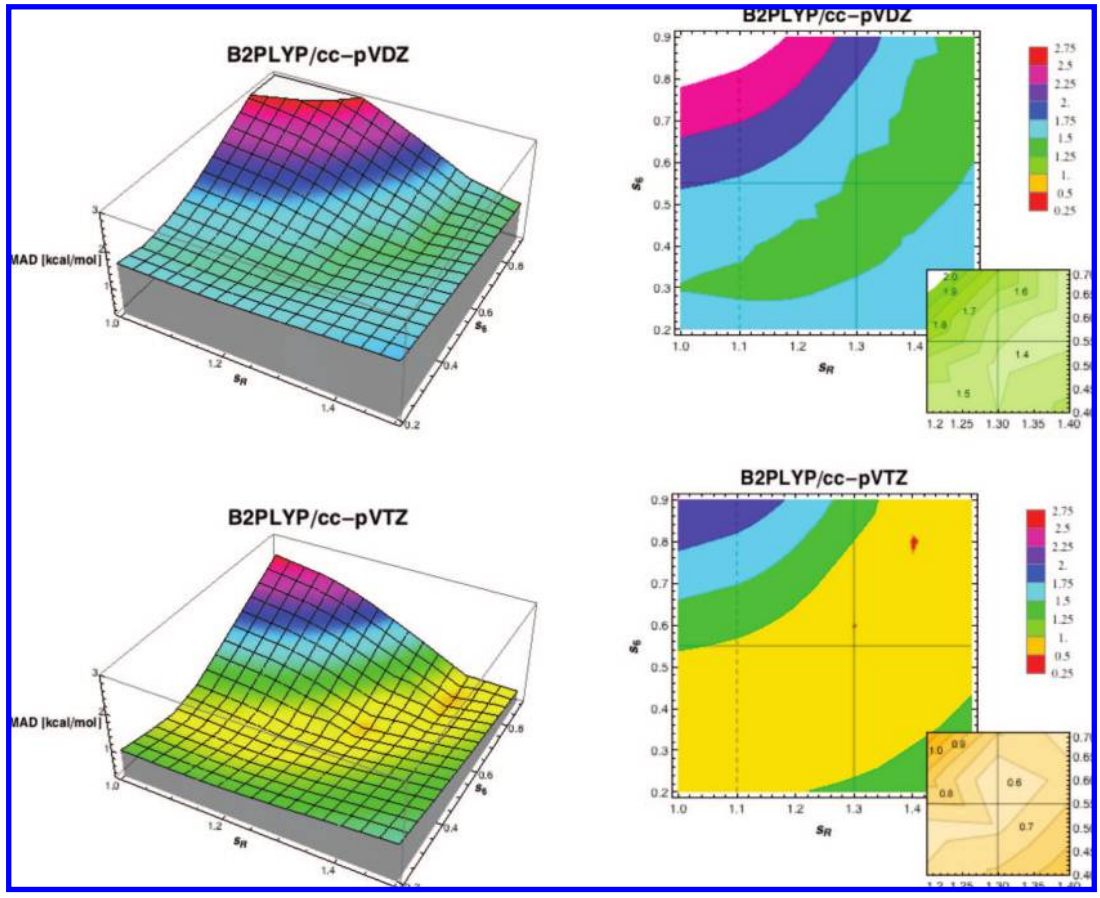

Figure 4. Optimized s_6 and s_R empirical dispersion function parameters for the B2PLYP double-hybrid functional, with the cc-pVDZ (top) and cc-pVTZ (lower) basis sets. Plots are shown using the same relative scale as those shown in Figures 2 and 3. Inset graphs are provided showing the minimum region in more detail.

shown as solid lines and the optimized values of Grimme are shown as dotted lines in the graphics.

Further Considerations of Basis Sets and BSSE. Following the above analysis, we proceeded to optimize the s_6 parameter for several additional functionals and basis sets, keeping the s_R value fixed to 1.1, as also suggested in the original paper of Grimme, given that this choice looks consistent also for the basis sets and functional types considered here. The first functional considered was the B97D exchange-correlation functional.[24] The cc-pVnZ basis sets (with $n = 2-4$) were used to investigate the behavior of the optimized s_6 parameter for increasing value of ζ (n). In addition, the reference TZV(2d,2p) optimized parameter of 1.25 was also considered.

Figure 5 shows the median absolute deviation (MAD) for the S22 set of molecules, with respect to increasing s_6 value, using the B97D functional. The optimized s_6 parameter increases with the addition of every ζ (n) to the basis set, as expected. With small basis sets ($n = 2$), one expects the basis set superposition error, BSSE, to be significant. The triple-ζ

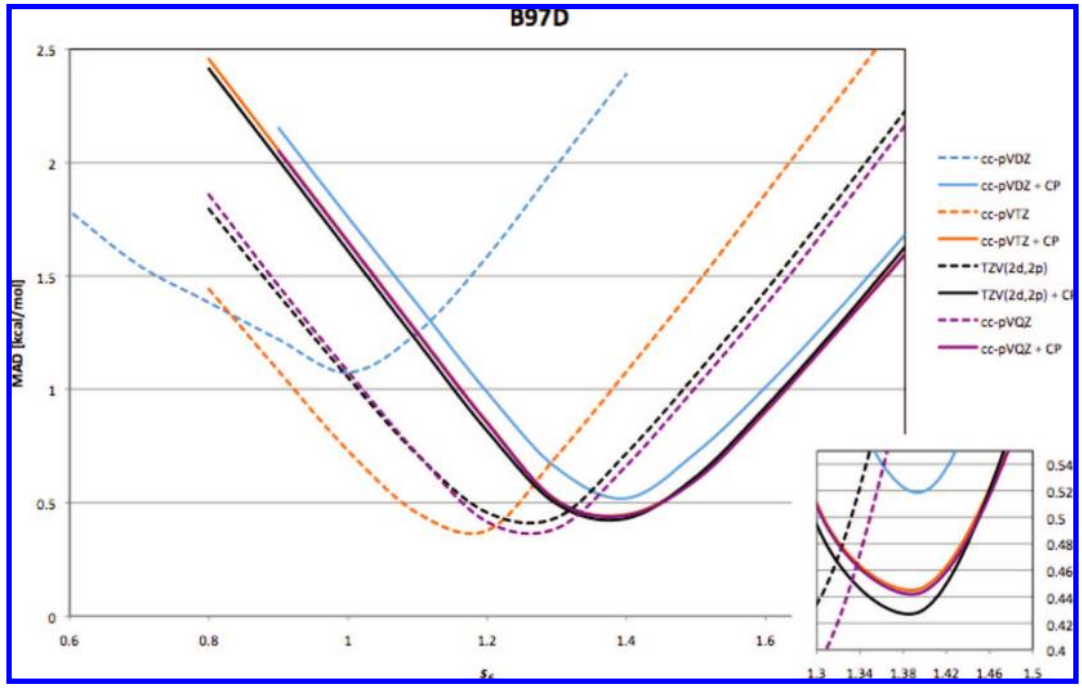

Figure 5. Median absolute deviation (MAD) with respect to increasing s_6 value, for the B97D functional. A detailed view of the minimum region is also provided for the CP corrected curves.

basis sets have almost the same overall performance as the higher-order quadruple-ζ basis set, with MAD lower than 0.5. The cc-pVTZ basis set, with optimized s_6 parameter of 1.18, has a slightly better overall performance than does the TZV(2d,2p) basis set. Indeed, the original TZV(2d,2p)-optimized parameter of 1.25 of Grimme provides acceptable errors of around 0.5 with the cc-pVTZ basis set. This fact suggests that a reoptimization of the s_6 parameters with basis sets that contain the same number of split shells is not really necessary, while the reduction of the number of split shells (i.e., from triple to double-ζ) can involve a significant increase in BSSE that must be compensated by a corresponding reduction of the optimized s_6 parameters.

The basis set superposition error (BSSE) plays a key role in the understanding of weakly bounded complexes interaction energies. It is well-known that basis sets that are too small will have large BSSE, resulting in poor binding energies and intermolecular distances.[40] Although it has been shown that DFT is much less affected by BSSE than other wave function types, a basis set of at least triple-ζ quality is necessary to significantly reduce the BSSE. The counterpoise correction (CP) is the standard method to correct for BSSE, and while the procedure itself has an associated error (typically results in an overestimation of BSSE) and requires additional effort, it typically provides good results for the vast majority of cases where it is used.

When the semiempirical-corrected DFT methodologies are employed, optimized parameters inherently account for part of the BSSE, as pointed out in the literature.[24,71] In fact, for small basis sets, BSSE can be of the same order of magnitude as the dispersion corrections; however the two corrections have different asymptotic behavior. To better understand the behavior of dispersion corrections and BSSE with respect to basis set and functional variations, we have performed parameter optimization with and without the CP correction. In Figure 5, the optimization of the s_6 parameter for the B97D functional including counterpoise correction is shown for several basis sets. Interestingly, the CP curves for all basis sets considered have a minimum at $s_6 = 1.4$ (general value that we suggest to use when CP corrections are applied with B97D), a quite large value compared to the ones for non CP-corrected curves. Since we can reasonably expect BSSE for large basis (e.g., cc-pVQZ) to be almost completely reduced to zero, one would expect the optimal s_6 value for the CP-corrected curves to be in the same region, but this is not the case.

Looking at the global performance in terms of MAD of the S22 set, one can see that the MAD is correctly reduced on going from cc-pVnZ to cc-pVnZ + CP for $n = 2$, but slightly increases for $n > 2$ (where the BSSE should be very small also for the noncorrected basis). The loss of accuracy within the same basis set has to be attributed to the error associated with the CP corrections, since no other source of errors are introduced in the calculations. This difference should actually be a reasonable energetic estimate of the error associated with the CP procedure within the S22 set of molecules. Given a much larger database of molecules, this procedure should be a way to quantify the global performance of the CP methods, something that will be considered in future work.

Similar considerations can be made for the B3LYP, PBE, and revPBE functionals. Parameter optimizations were performed and results collected in Figures 6−8.

The optimal s_6 parameters show the same behavior for all three functionals, resulting in an increase of this parameter value with dimension of basis set. The revPBE functional actually shows a relatively strange overall performance: its accuracy is in fact reduced with increase in basis set, with the double-ζ basis set having the lowest MAD value. To better analyze the s_6 optimization process,

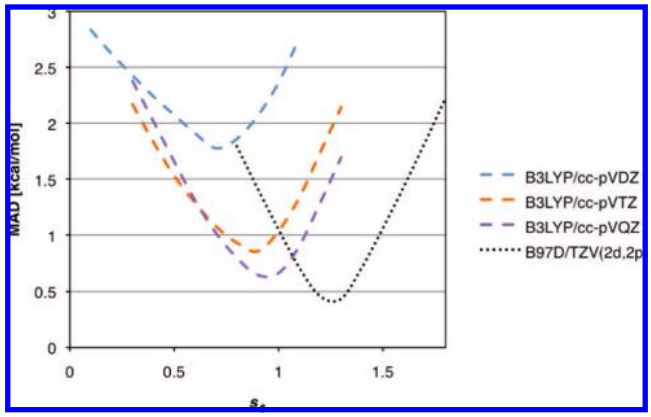

Figure 6. Optimization of the s_6 and s_R parameters for the B3LYP functional at cc-pVnZ, $n = 2-4$, compared to the B97D functional at the TZV(2d,2p) basis set with optimized $s_6 = 1.25$.

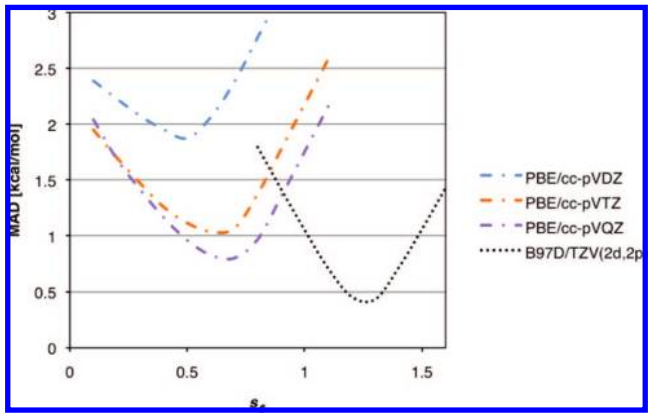

Figure 7. Optimization of the s_6 and s_R parameters for the PBE functional at cc-pVnZ, $n = 2-4$, compared to the B97D functional at the TZV(2d,2p) basis set with optimized $s_6 = 1.25$.

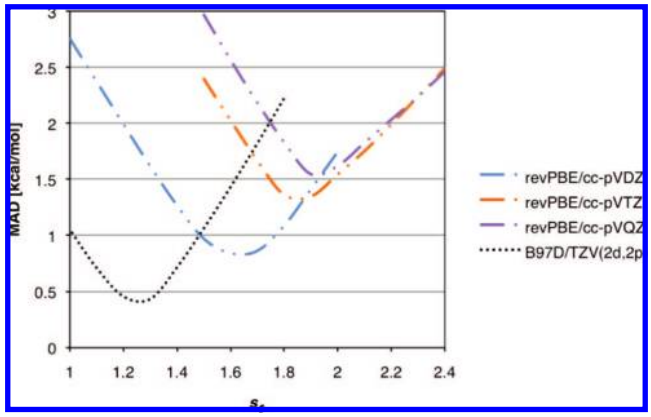

Figure 8. Optimization of the s_6 and s_R parameters for the rev-PBE functional at cc-pVnZ, $n = 2-4$, compared to the B97D functional at the TZV(2d,2p) basis set with optimized $s_6 = 1.25$.

the deviation from reference for cc-pVDZ with the nonoptimized and optimized s_6 values for the S22 set of complexes was investigated, in addition to results of DFT without dispersion (Figure 9−13).

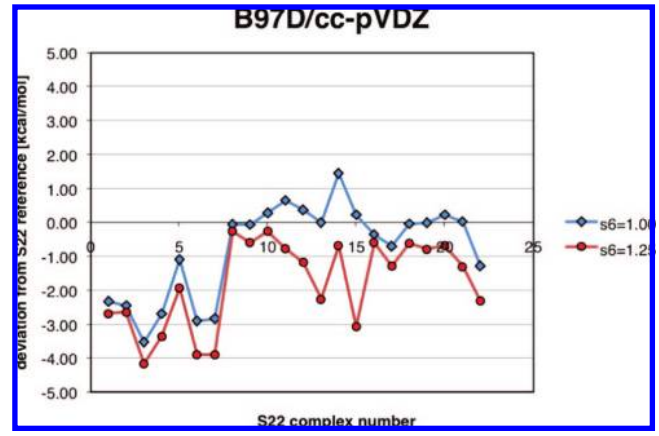

Figure 9. Deviation of DFT+D calculated and CCSD(T) reference at $s_6 = 1.25$ vs $s_6 = 1.00$ for the S22 set of complexes for B97D/cc-pVDZ.

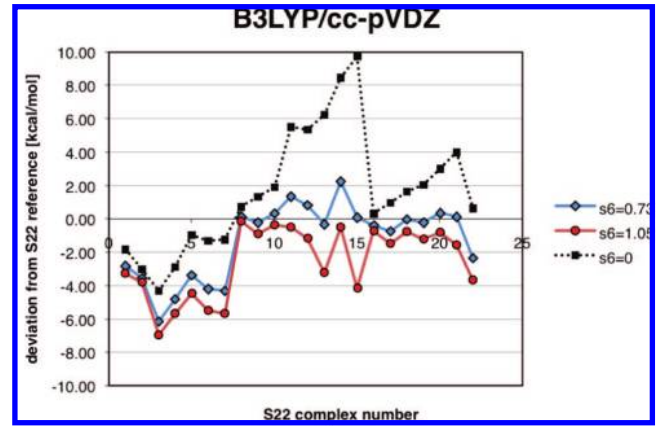

Figure 10. Deviation of DFT+D calculated and CCSD(T) reference at $s_6 = 1.05$ vs $s_6 = 0.73$ for the S22 set of complexes for B3LYP-D/cc-pVDZ.

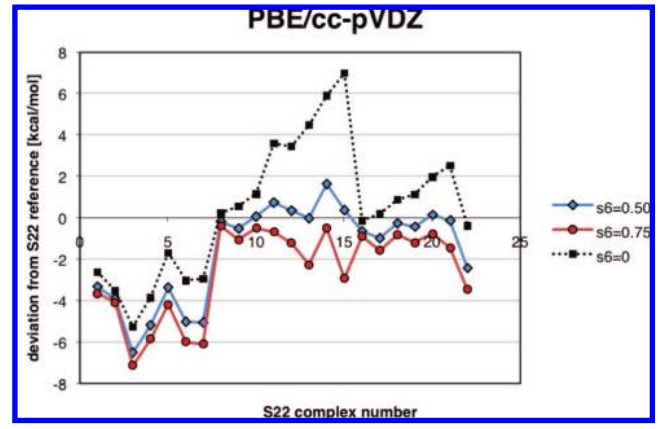

Figure 11. Deviation of DFT+D calculated and CCSD(T) reference at $s_6 = 0.75$ vs $s_6 = 0.5$ for the S22 set of complexes for PBE-D/cc-pVDZ.

As can be expected, one observes the general improvement of results with inclusion of the dispersion correction (DFT vs DFT-D results). The largest errors for DFT-D are found for the first 7 complexes in the S22 set, which are all hydrogen-bonded complexes. Complexes 8−15 have predominantly dispersion contributions, while complexes 16−22 involve more complicated diverse interactions. In the case

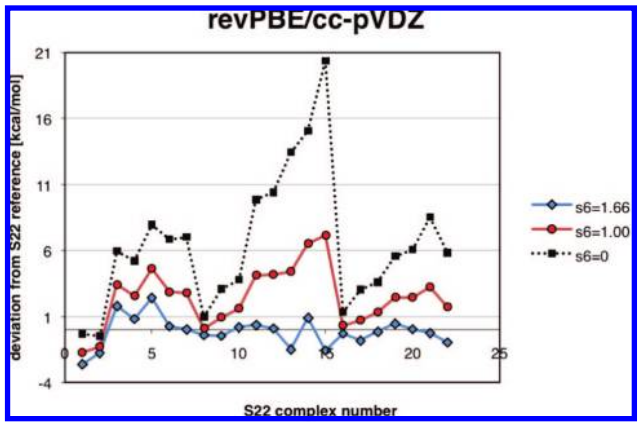

Figure 12. Deviation of DFT+D calculated and CCSD(T) reference at $s_6 = 1.66$ vs $s_6 = 1.00$ for the S22 set of complexes for rev-PBE-D/cc-VDZ.

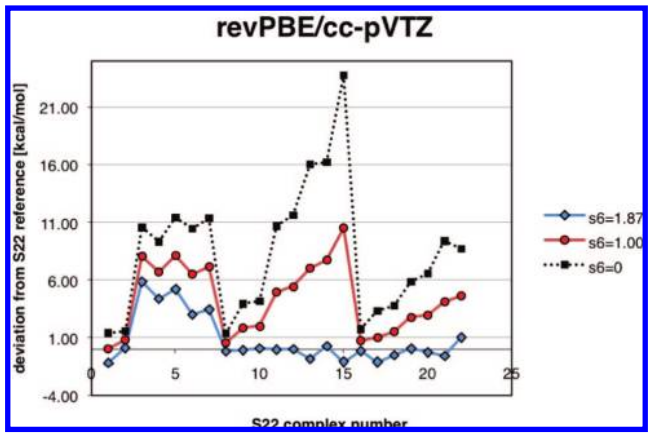

Figure 13. Deviation of DFT+D calculated and CCSD(T) reference at $s_6 = 1.87$ vs $s_6 = 1.00$ for the S22 set of complexes for rev-PBE-D/cc-VTZ vs rev-PBE/cc-pVTZ.

of PBE and revPBE, the optimized values sensibly flatten the curve in the pure dispersion and in the mixed regions, while maintaining acceptable results in the hydrogen-bonded area.

The apparently strange behavior of revPBE with respect to basis set increase can be rationalized through a comparison of the plot in Figure 12 for cc-pVDZ with a corresponding plot for cc-pVTZ shown in Figure 13. While errors for complexes 8−22 are satisfactorily reduced for the triple-ζ basis set, errors associated with the hydrogen bond complexes (complexes 1−7) are actually increased, reducing the global performance (MAD) for this functional. The MAD of complexes from 8−22 using revPBE/cc-pVTZ and revPBE/cc-pVQZ is on the same order of that obtained for B97D using the same respective basis sets, as can be seen in Table 1.

Figure 14 shows all results together, illustrating the performances of the different functionals. The B97D with triple-ζ basis set appears to be in general the best choice for accurate calculations. Interestingly, B97D with cc-pVDZ provides essentially the same performance as B3LYP-D with cc-pVTZ. Oddly, the results of revPBE/cc-pVDZ appear to provide the overall best of the other double-ζ basis sets (Figure 15) and, additionally, of nearly all triple-ζ basis sets and even some of the quadruple-ζ basis sets. However, as

Table 1. Mean Absolute Deviation of S22 Complexes for the Series of Functionals and Corresponding Basis Sets for the Optimized s_6 Values Shown

DFT functional	basis set	optimized s_6 value	MAD (kcal/mol)
B97D	cc-pVDZ	1.00	1.075
	cc-pVDZ + CP	1.39	0.518
	cc-pVTZ	1.18	0.337
	cc-pVTZ + CP	1.41	0.454
	cc-pVQZ	1.26	0.330
	cc-pVQZ + CP	1.39	0.441
	TZV(2d,2p)	1.25	0.375
	TZV(2d,2p) + CP	1.38	0.425
B3LYP	cc-pVDZ	0.73	1.709
	cc-pVTZ	0.88	0.853
	cc-pVQZ	0.96	0.612
PBE	cc-pVDZ	0.50	2.579
	cc-pVTZ	0.64	1.030
	cc-pVQZ	0.65	0.798
revPBE	cc-pVDZ	1.66	0.826
	cc-pVTZ	1.87	1.326
	cc-pVQZ	1.90	1.536
	cc-pVTZ (8−22)	1.87	0.393
	cc-pVQZ (8−22)	1.90	0.355

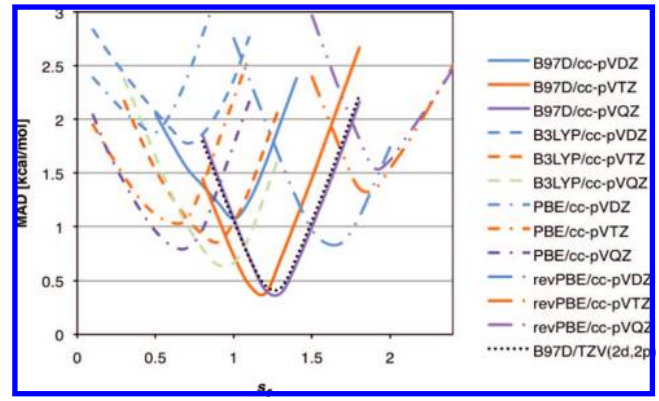

Figure 14. Mean absolute deviation at optimal s_6 values for the functionals and basis sets considered in this study.

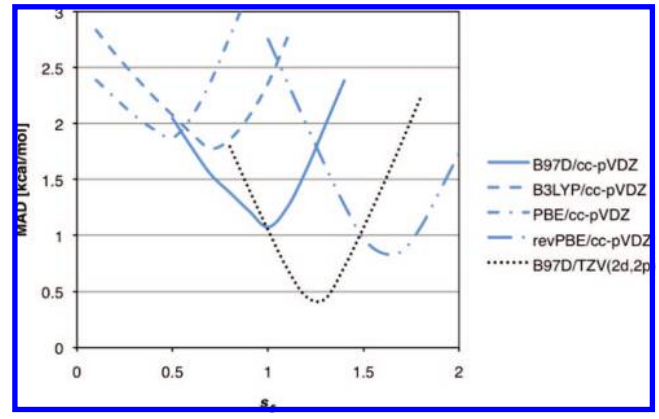

Figure 15. Mean absolute deviation at optimal s_6 values for functionals using the cc-pVDZ basis set as compared to B97D/TZV(2d,2p).

we observe when applying this functional, these results are a bit misleading because results for structure and properties of molecules outside the S22 test set are found to be not as good as with, for example, the B97D functional. The high values of the optimal s_6 for the revPBE functional are

Table 2. Summary of DFT-D Results As a Function of Basis Set and CP Correction for Methane Dimers

	$(CH_4)_2$ D_{3h} (eclipsed)			$(CH_4)_2$ D_{3d} (staggered)	
method	s_6	ΔE (kcal/mol)	R_e (Å)	ΔE (kcal/mol)	R_e (Å)
B97D/TZV(2d,2p)	1.25			−0.567	3.792
B97D/TZV(2d,2p) + CP	1.25			−0.558	3.792
B97D/cc-pVDZ	1.25	−0.743	3.600	−0.782	3.606
B97D/cc-pVDZ + CP	1.25	−0.527	3.600	−0.558	3.606
B97D/cc-pVDZ opt	1.00	−0.521	3.747	−0.548	3.792
B97D/cc-pVDZ + CP opt	1.39	−0.882	3.595	−0.924	3.518
B3LYP-D/cc-pVDZ	1.25	−0.778	3.411	−0.830	3.409
B3LYP-D/cc-pVDZ + CP	1.25	−0.518	3.411	−0.545	3.409
B3LYP/cc-pVDZ		unbound		unbound	
B3LYP/cc-pVDZ + CP					
Grimme[a]				−0.56	3.78
experiment[b]				−0.33 to −0.46	3.84 to 4.27

[a] Ref 24 [b] Experimental range of values from refs 76−81. Counterpoise (CP).[82,83]

evidence that the exchange part of this functional correctly provides little to no bond in the vdW region, forcing the vdW interactions to be treated by the semiempirical dispersion-like term. For this reason and because of its simple GGA implementation and large use in physical and surface science, revPBE/cc-pVDZ appears to be one of the best reference methods for large systems. The B97D functional is still a very good choice using either double-ζ or triple-ζ basis sets, given its rational balance of exchange and correlation terms, and over all good behavior in general. For use with the cc-pVDZ basis set, a sensible reduction of the optimized s_6 parameter is necessary.

To further validate results, we also looked at small molecule benchmark dimers that have been used in many other investigations of this type, some of our larger models for aryl/aryl interactions, as well as corannulene constructs, given the large focus on these latter systems in our research. The first two small but nontrivial tests include methane dimers and benzene dimers, the latter of which has been the subject of many experimental and theoretical investigations for which there is considerable benchmark data. In addition to all of the above-mentioned functionals, for the research applications, we include results from a recent implementation of the M06 series of functionals of Zhao and Truhlar into GAMESS by Sok.[75]

Methane Dimers. $(CH_4)_2$ in D_{3d} (staggered) conformations was first considered using B97D/TZV(2d,2p) to verify in accord with literature[24] and experimental results. [76−81] Counterpoise (CP) [82,83] corrections for basis set superposition error (BSSE) were also investigated for both, the summary of which is in Table 2.

Results for the staggered conformation of the methane dimer are in good agreement with those of Grimme, as well as experimental data. Small differences from that of Grimme can be attributed to (a) Grimme using a resolution of the identity RI approximation for two-electron integrals, and (b) a slight difference in basis set: Grimme uses TZV2P basis set[62] (discarded d- and f- function on first and 2−5-row atoms, respectively); here TZV(2d,2p)[84] as implemented in GAMESS is used.

As previously mentioned, counterpoise corrections need to be treated with caution because such effects are partially accounted for within the semiempirical dispersion correction itself. At the double-ζ, such considerations may still be required, but one should be aware that the semiempircal correction might influence the effectiveness of the CP treatment. One immediately sees that B3LYP+CP is very poor, actually predicting methane dimer to be unbound. In contrast, the addition of the semiempirical dispersion correction overshoots the mark, predicting the methane monomers to be too close and too strongly bound. B97D/cc-pVDZ actually does a comparable job to the larger basis set with the inclusion of CP, albeit again, slightly over bound. Ultimately, the study indicates the need for at least triple-ζ whenever feasible, but that the B97D functional does a reasonable job even for double-ζ.

Benzene Dimers. Although benzene dimer structures can adopt a continuum of different relative orientations, three prototype structures are typically considered, parallel-stack (PS), parallel-offset (PO), and edge-to-face (EF) (Table 3). Whereas the PO and EF are stable minima, the PS is a transition state structure. Two important considerations in these dimers is the balance between contact surface (CS) and polar moment (PM). The polar moment overlap in PS is much larger than in the other two cases, resulting in maximum repulsive polar moment. In the PO structure, the two contributions are quite similar and offer moderate attraction between the two benzenes, while the EF structure has minimal attraction with the contact surface compared to the much larger polar moment attraction.

It is well-known that nondispersive DFT functionals, in particular the popularly exploited B3LYP, give a purely repulsive interaction for the PO configuration of the benzene dimer. Our goal in this work is to see how the DFT-D methods discussed above perform for this complex. The best theoretical estimate of the interaction energy for the PS conformation has been provided by Sinnokrot and Sherrill, at the CCSD(T)/aug-cc-pVQZ* (modified basis set) level of theory,[85] enabling us to compare complete dissociation curves.

Here we have investigated the B3LYP-D, B97D, PBE-D, and revPBE-D, with optimized s_6 parameters for the cc-pVDZ basis set. While it is true that one would choose a more substantial basis set for this small system, our goal is to determine feasibility of double-ζ level basis sets for the

Table 3. Relative Relationship between Contact Surface and Polar Moment in Benzene Dimer Structures

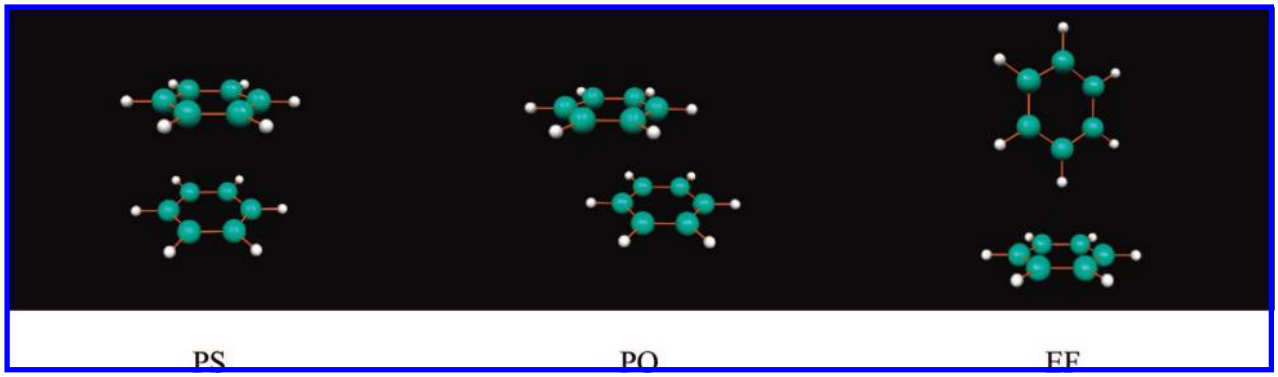

conformation	contact surface (CS)	polar moment (PM)	relative relationship
PS	maximum attraction	repulsive	CS < PM
PO	medium attraction	attractive	CS ≈ PM
EF	minimum attraction	attractive	CS ≪ PM

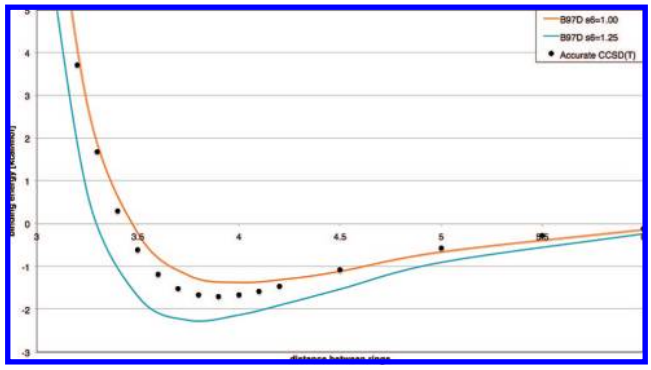

Figure 16. B97D-D/cc-pVDZ energy as a function of intermolecular distance for the benzene face-to-face dimer complex, with $s_6 = 1.0$ and $s_6 = 1.25$, compared to the CCSD(T) reference curve, as explained in the text.

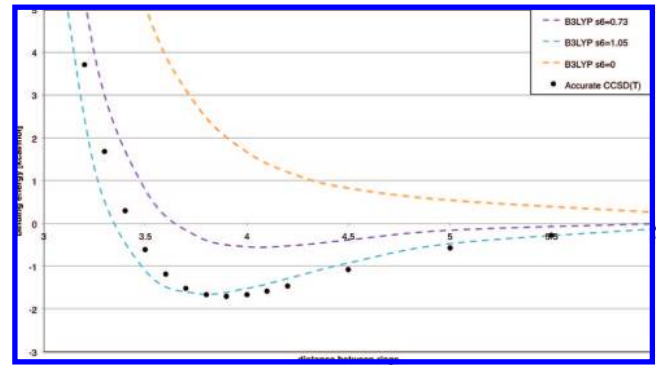

Figure 17. B3LYP-D/cc-pVDZ energy as a function of intermolecular distance for the benzene face-to-face dimer complex, with $s_6 = 1.05$ and $s_6 = 0.73$, and no dispersion correction, compared to the CCSD (T) reference curve, as explained in the text.

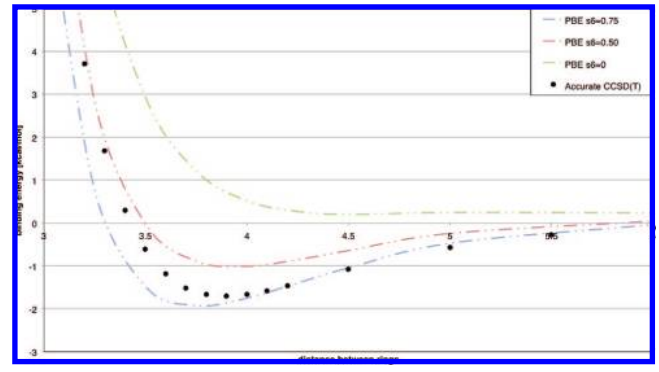

Figure 18. PBE-D/cc-pVDZ energy as a function of intermolecular distance for the benzene face-to-face dimer complex, with $s_6 = 0.75$ and $s_6 = 0.50$, and no dispersion correction, compared to the CCSD(T) reference curve, as explained in the text.

purpose of extending these methods to significantly larger aryl/aryl systems shown below. Full dissociation curves have been computed for each of the four functionals. These dissociation curves, in comparison to the high quality curve of Sherrill and Sinnokrot, provide a better understanding of how the methods appropriately reproduce the strength of the $\pi-\pi$ interactions as a function of distance and orientation of the rings. All curves have been constructed using single-point energy calculations of the dimer at variant intermolecular benzene-benzene distance, using experimental benzene internal geometry. Results are shown Figures 16−19 for the different functionals.

Of the functionals investigated, the B97D functional appears to be one of the better functionals for prediction of the interaction energy profile for the benzene dimer, keeping in mind that the optimization of the s_6 parameter plays a key role when moving from double-ζ to higher-order basis sets. For the popularly used B3LYP functional, we note the anomaly that the nonoptimized curve ($s_6 = 1.06$) has a better behavior than the optimized curve, primarily because of a cancelation of errors. The s_6 optimization for the PBE functional does not have a particularly large influence on single-point energies at experimental equilibrium geometries. Even if the single-point energy looks worse, the minimum of the optimized curve is nearly predictive of the experimental optimal distance, while the nonoptimized curve predicts overbinding. The two PBE-based functionals have globally acceptable results, with errors reduced from 6 kcal/mol using unoptimized s_6 to almost 2 kcal/mol when used

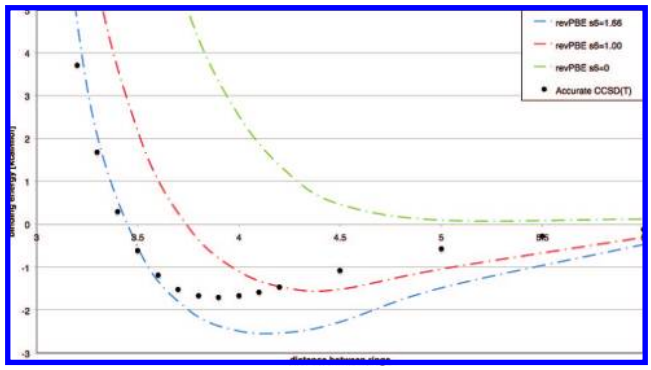

Figure 19. revPBE-D/cc-pVDZ energy as a function of intermolecular distance for the benzene face-to-face dimer complex, with $s_6 = 1.66$ and $s_6 = 1.0$, and no dispersion correction, compared to the CCSD(T) reference curve, as explained in the text.

with the optimized s_6 parameters. This supports considerations of its general use for significantly large systems.

The best estimate of the interaction energy for the PS conformation, evaluated at the equilibrium intermonomer distance, is provided by the CCSD(T)/aug-cc-pVQZ* (modified basis set) potential energy curve of Sinnokrot and Sherrill, at −1.70 kcal/mol. For reference, their MP2/aug-cc-pVDZ and CCSD(T)/aug-cc-pVDZ numbers are −2.83 and −1.33 kcal/mol, respectively. The experimental dissociation of the benzene dimer, determined by Grover in 1987, is found to be in the range of −2.0 to −2.8 kcal/mol.[86] Here, as seen above with the methane dimers, the B3LYP-D functional performs quite poorly. However, using the B97D functional, we obtain −1.70 kcal/mol with TZV(2d,2p) and optimized s_6 values of Grimme (−1.559 including CP) and −1.34 kcal/mol using our optimized s_6 values for cc-pVDZ, in very close agreement to that obtained with the CCSD(T)/aug-cc-pVDZ, −1.33.

Research Applications. There is considerable interest, both from an experimental and a theoretical perspective, of alkyl−π and aryl−π interactions because of their importance in many applications from materials to biological systems. Many such studies predict (a) that dispersive forces dominate the interaction, (b) a repulsive nature of the PS and an attractive nature of the PO and EF, and (c) that electron-donating (ED), as well as electron-withdrawing (EW), groups enhance stacking interactions.[87−91] Experimental evidence for the repulsive interaction in the PS conformation has been demonstrated by Siegel and Cozzi through a number of investigations[92−95] of substituted 1,8-diarylnapthalenes and confirmed by others, [96,97] which aid in the rationalization of a variety of other experimental results in different fields. Experimental evidence for the EF conformation, involving the interaction between the CH groups of the edge ring and the π electron density of the face ring, has been less conclusive, some indicating sensitivity to changes in the local charge distribution on the rings and others finding no particular sensitivity.

Experimental studies, again by Cozzi and Siegel, together with our theoretical contributions, focused on the PO conformation in two conformationally restricted polycyclic systems[98] and showed that through-space interactions between PO oriented arenes is strongly influenced by electrostatic effects. Therefore, because these same interactions are important in EF and PS structures, polar−π interactions are seen to be a decisive factor for understanding arene−arene interactions.

In more recent theoretical investigations, together with the experimental groups of Siegel and Cozzi, [99] we proposed a model for systematic investigation of a PO geometry polar−π interactions between arenes spaced at vdW distances, enabling us to provide a direct comparison of experiment and theory across different functional group modifications. A set of 1,8-diarylbiphenylene comprising two Hammett series was investigated (Figure 20). The model provides an excellent test to compare the sensitivity of DFT models to pick up appropriate polar−π interactions between the two arenes. In particular, compare the following functionals: B97D, BMK, M06−2X, and B3LYP. Results are shown for the cc-pVDZ basis set, however, triple-ζ, additional polarization and diffuse functionality were also investigated, with no significant change in the following trends. The following substituents were considered: OMe, H, Cl, and F. Two possible ground-state conformations are possible corresponding to a slight canting of the aryl groups such that the methyl of the probe ring is either endo or exo. All derivatives tend to adopt the endo conformation by ∼2−5 kJ/mol, consistent with crystallographic forms found for this series.

In the previous work, we found a distinctly better performance of BMK for predicting geometry in the entire series across ten geometric parameters used to describe this interarene interaction. Table 4 reports calculated results across these 10 geometric parameters for the substituents X = OMe, H, Cl, and F, using our B97D implementation. In addition, the barriers to rotation of the probe aryl ring are determined and compared to experimental values that are derived from dynamic NMR data. The critical distances *a*, *b*, *c*, and the interplanar (ip) stacking distance, in particular, show how the different functionals respond to the polarizability and vdW effects.

A regression analysis of experiment versus theory for X = H, Cl, and F shows excellent prediction, with regression coefficients of $R = 0.9988$, $R = 0.9999$, and $R = 0.998$, respectively. The largest errors occur in the case of X = H and X = F, for the parameters ϕ and φ, which are associated with the canting of the rings with respect to each other. All barriers are predicted to be within 1.3 kcal/mol of the reported experimental values.

Results of a comparison across four density functionals for two of the substituted diarylbiphenylenes, X = H and X = Cl, was also carried out (Table 5a). The B3LYP functional shows the largest deviation from experimental values in both cases as expected. The interaction between the aryl rings is underestimated interaction as reflected in the greater distance found between the two aryl rings, and the small barrier to rotation of the probe ring. In the opposite extreme is M06−2X, which overestimates the interaction resulting in aryl rings that are too close and in barrier to rotation that is too large. The BMK functional provides very good agreement with experiment. The newest addition, B97D, is very close to the BMK results, the major difference being the amount

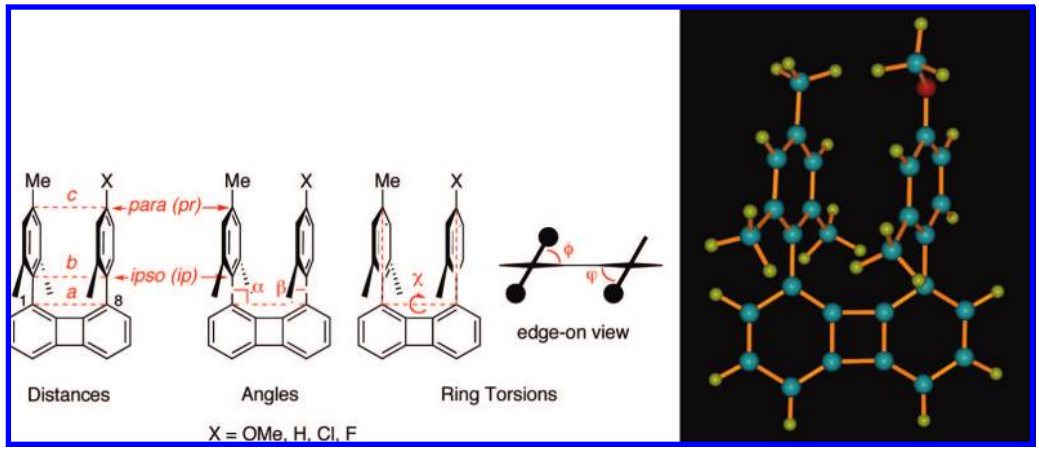

Figure 20. a) peri-Substituted biphenylene as a model for PO benzene dimers. (b) Representative OMe-substituted biphenylene.

Table 4. B97D/cc-pVDZ Structure and Rotational Barrier Results for the Set of 1,8-Diarylbiphenylenes with Substitutents X = OMe, H, Cl, and F

	X = OMe	X = H		X = Cl		X = F	
parameter	calcd	calcd	exptl	calcd	exptl	calcd	exptl
a (Å)	3.8168	3.8251	3.80(1)	3.8262	3.773(6)	3.8260	3.797(5)
b (Å)	3.7962	3.8276	3.89(1)	3.8312	3.815(6)	3.8263	3.812(5)
c (Å)	3.6768	3.7442	3.84(1)	3.8532	3.776(6)	3.7146	3.715(5)
α (deg)	89.3	89.7	90.7(4)	89.8	90.3(2)	89.8	90.3(1)
β (deg)	89.7	90.3	92.3(4)	90.3	91.2(3)	90.1	90.3(1)
ϕ (deg)	60.1	62.8	61.0(9)	62.8	62.1(6)	62.7	65.8(3)
ψ (deg)	56.9	59.4	65.1(9)	59.5	59.2(7)	58.6	65.8(3)
χ (deg)	8.1	2.8	3.0(2)	2.9	3.7(1)	2.8	2.4(1)
$ip_\perp$ (Å)[a]	3.42	3.43	3.595(6)	3.40	3.456(4)	3.42	3.544(2)
$pr_\perp$ (Å)[a]	3.46	3.39	3.607(7)	3.46	3.481(4)	3.43	3.490(3)
barrier[b]	11.6	10.9	9.7	10.9	10.1	11.9	10.6

[a] $ip_\perp$ and $pr_\perp$ = orthogonal distance from *ipso*- or *para*-carbon of reference ring to mean plane of probe ring, respectively. [b] Experimental determinations were performed in solvent.

of canting of one ring with respect to each other, and the predicted barriers for the former are slightly higher. The interplanar distances $ip_\perp$ and $pr_\perp$ are predicted to be on average 3.4 for both BMK and B97D, which is what is found experimentally, because this parameter is relatively constant over the series of functional modifications. Figure 21 illustrates this phenomenon in an overlay of all four functional predictions for the X = Cl substituted compound. Here, one can clearly see the difference in association of the two aryl rings using the different functionals. Table 5b shows the deviations from experimental results across the entire set. Across all parameters, the B97D provides a uniform agreement with experimental results for all substituents, providing a high degree of predictability. The largest error is, again, associated with the tilt angle of the two rings with respect to each other.

Corannulene. Corannulene as a shallow bowl structure undergoes a dynamical bowl inversion process. The bowl inversion relates two symmetry-equivalent minima through a common flat structure transition state. Our previous investigations[9] involving systematic study of the differences in bowl-inversion barriers and bowl depth for a variety of substituted corannulene derivatives established a predictive structure−energy correlation, wherein deeper bowl depth gives rise to higher inversion barrier and vice versa. This correlation, $\Delta E = -a(x_{eq})^4$, leads to a quartic relationship between the inversion energy (ΔE) and equilibrium bowl depth (x_{eq}) and holds for a large subset of corannulene derivatives.

As is well established, the B3LYP/cc-pVDZ level of theory happens to provide highly accurate predictions of structural parameters of corannulene and substituted derivatives as compared to experiment; however, it significantly underestimates the barrier to inversion. Møller−Plesset perturbation theory of order 2 (MP2) carried out at the optimized B3LYP/cc-pVDZ geometry enables accurate predictions of the barrier. This protocol is reliable for many functionalized corannulene derivatives and appears to be only compromised when secondary structural interactions in specific derivatives, such as additional vdW interactions, can occur.

We have investigated the sensitivity of various density functionals with regard to structure and properties of corannulene, including the simple local density approximation (LDA) of SVWN, several GGAs, such as BP86, BLYP, PBE, PBE0, several meta-GGA's and hybrid methods, such as X3LYP, PW91, and most importantly, for the structures with secondary interactions, the series of B97 functionals and the BMK and M06−2X functionals. We have added dispersion corrections to many of these functionals (indicated here with the appended "-D" notation), using optimized scale-factors (Table 6), and tested them out on the corannulene structure and dynamics.

Table 5. (a) Structural and Rotational Barrier Results and (b) Structural and Rotational Deviations from Experimental Results for a Subset of 1,8-Diarylbiphenylenes with Substitutents X = H and Cl

(a)

	X = H				X = Cl			
parameter	B3LYP	M06−2X	BMK	B97D	B3LYP	M06−2X	BMK	B97D
a (Å)	3.8699	3.7948	3.8357	3.8251	3.8637	3.7949	3.8291	3.8262
b (Å)	4.0547	3.7677	3.8915	3.8276	4.0177	3.7620	3.8483	3.8312
c (Å)	4.5661	3.6614	4.0101	3.7442	4.3911	3.6316	3.7800	3.8532
α (deg)	93.3	88.6	90.9	89.7	92.7	89.3	90.4	89.8
β (deg)	93.8	90.3	91.2	90.3	93.2	89.4	90.3	90.3
ϕ (deg)	71.1	63.5	65.4	62.8	71.1	63.7	65.5	62.8
ψ (deg)	68.1	61.1	61.6	59.4	67.8	60.2	60.7	59.5
χ (deg)	0.2	1.4	2.1	2.8	0.6	2.0	1.6	2.9
$ip_{\perp}$ (Å)	3.76	3.51	3.38	3.43	3.75	3.47	3.37	3.40
$pr_{\perp}$ (Å)	4.22	3.63	3.30	3.39	4.08	3.40	3.27	3.46
barrier	8.8	12.9	9.8	10.9	8.7	13.4	10.0	10.9

(b)

	3b (X = H)				3d (X = Cl)			
parameter	B3LYP	M06−2X	BMK	B97D	B3LYP	M06−2X	BMK	B97D
a (Å)	0.0689	−0.0062	0.0347	0.0241	0.0901	0.0213	0.0555	0.0526
b (Å)	0.1637	−0.1233	0.0005	−0.0634	0.2021	−0.0536	0.0327	0.0156
c (Å)	0.7251	−0.1796	0.1691	−0.0968	0.6145	−0.1450	0.0034	−0.0766
α (deg)	2.6	−2.1	0.16	−1.0	2.4	−1.0	0.10	−0.50
β (deg)	1.5	−2.0	−1.14	−2.0	2.0	−1.9	−0.94	−0.91
ϕ (deg)	10.0	2.4	4.3	1.7	9.0	1.6	3.3	0.68
ψ (deg)	2.9	−4.1	−3.6	−5.8	8.9	0.9	1.5	0.24
χ (deg)	−2.8	−1.6	−0.92	−0.22	−3.1	−1.8	−2.1	−0.77
$ip_{\perp}$ (Å)	0.16	−0.08	−0.21	−0.16	0.29	0.01	−0.09	−0.05
$pr_{\perp}$ (Å)	0.61	0.02	−0.31	−0.22	0.60	−0.08	−0.21	−0.01
barrier	−0.90	3.2	0.10	1.2	−1.3	3.3	−0.10	0.80

The high degree of symmetry of corranulene makes it difficult to obtain a precise experimental value for the barrier to the bowl-to-bowl inversion process, but it has been estimated from a series of functionalized structures to be about 11.5 kcal/mol. The best theoretical estimate to date is 11.1 kcal/mol, at MP2/cc-pVDZ//B3LYP/cc-pVDZ, including ZPE. The ability to accurately estimate the barrier is directly related to the ability to accurately predict the structural parameters because of the known structure/energy correlation of bowl depth and inversion barrier. While the bond lengths and angles are quite well reproduced with respect to the experimental predictions, the more difficult geometric feature seems to be the bowl depth and curvature.

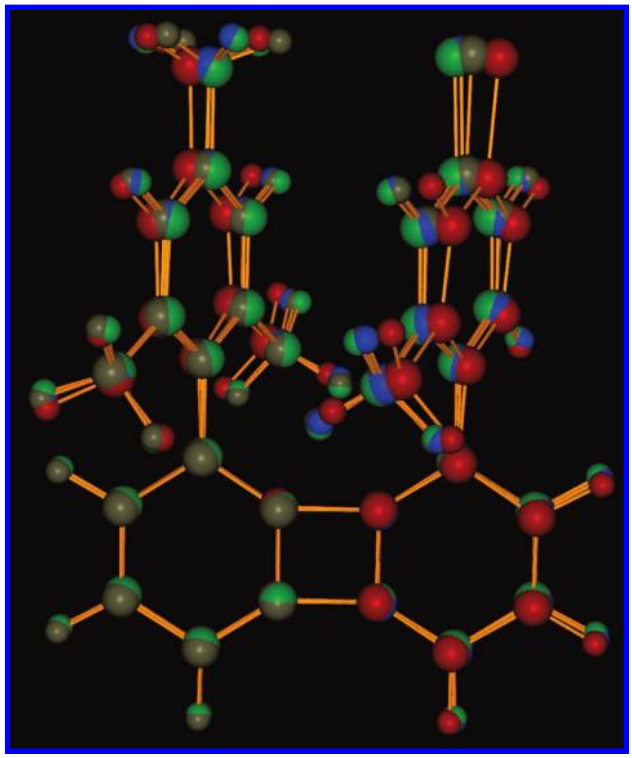

Figure 21. peri-Substituted biphenylene (X = Cl) for functionals B97D (brown), BMK (blue), M06−2X (green), and B3LYP (red).

As expected, the general functionals can be highly improved using dispersion corrections. The most noticeable difference in the results are a slight increase in bowl depth, resulting in an increase in barrier, as would be predicted from the established bowl/depth functional relationship. The best results are obtained with the B97D functional, which reaches the performance of the MP2 single point calculations for both reaction barrier and dipole moment predictions. Across all functionals, the barrier is still lower than the experimental value, although again, the experimental value is only an estimate because of the high symmetry of the molecule. The BMK functional gives surprisingly good performance across many functionalized corannulenes, as well as this unsubstituted case, likely, because of the high percentage of HF exchange with terms dependent on the kinetic energy density, suitable for describing the aromatic nature. The M06−2X functional provides quite good agreement with respect to the

Table 6. Barrier to Interconversion, Bowl Depth, and Dipole Predictions for Corannulene Using Various Density Functionals, and the cc-pVDZ Basis Set

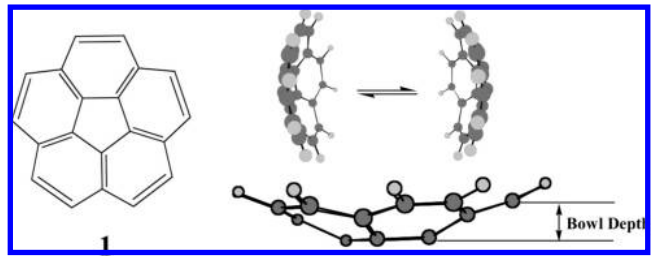

functional	ΔE^a (kcal/mol)	TS frequency (cm^{-1})	bowl depth (Å)	dipole (debye)	$-$(HOMO)^c (eV)
B3LYP	9.33 (9.21)	−109.1	0.87	1.88	6.0 (8.2)
MP2//B3LYP	11.12 (10.99)			2.29	
BLYP	8.74 (8.63)	−105.2	0.88	1.76	5.2 (6.7)
BP86	9.10 (9.09)	−107.9	0.89	2.00	5.6 (7.0)
PBE	9.41 (9.44)	−109.6	0.89	1.97	5.5 (7.0)
SVWN	9.98 (9.71)	−108.3	0.90	2.10	5.7 (7.2)
PBE0	9.50 (9.68)	−112.9	0.88	2.09	6.4 (8.8)
PW91	9.33 (9.31)	−108.9	0.89	1.94	5.5 (7.0)
X3LYP	9.09 (9.13)	−109.5	0.87	1.89	6.2 (8.4)
B97	9.19 (9.29)	−109.7	0.88	2.00	6.1 (8.2)
B97-1	9.25 (9.33)	−109.7	0.88	2.02	6.1 (8.3)
B97-2	9.56 (9.76)	−112.9	0.88	2.06	6.2 (8.4)
B3LYP-D	(9.96)		0.90	1.94	6.0 (8.2)
BLYP-D	(9.67)		0.91	1.82	5.2 (6.7)
BP86-D	(10.05)		0.92	2.07	5.6 (7.1)
PBE-D	(10.19)		0.91	2.00	5.5 (7.9)
revPBE-D opt	(9.55)		0.92	1.67	4.3 (5.8)
B97D	(10.39)		0.92	2.03	5.4 (6.9)
B97D opt	(10.10)		0.91	2.00	5.4 (6.8)
BMK	8.66 (8.84)	−104.0	0.88	2.14	6.9
M06−2X	9.98 (10.01)	−118.2	0.89	2.19	7.5
MP2/cc-pVDZ	9.11	−115.4	0.91	2.45	8.0
experiment	est. 11.5		0.87	2.071(18) ^{b}	8.37^c

^{a} Values in parenthesis are without ZPE. Hessians not yet available for dispersion functionals. ^{b} Ref 100 ^{c} While it has been shown that there is a correlation between HOMO eigenvalue and ionization potential, the absolute estimate is not a reliable measure of I.P. Values in parenthesis have been scaled according to the 3*HOMO - LUMO. Experimental IP is 8.37 eV and MP2/cc-pVDZ Koopmans Theorem=7.99 eV, ΔS CF=8.77 eV.[101]

experiment, although noticeably higher in many of the properties with respect to the other B97D functionals and BMK.

***sym*-1,3,5,7,9-Pentamanisylcorannulene.** Motivated by the deeper bowl depth and higher barrier to inversion, *sym*-1,3,5,7,9-pentamanisylcorannulene has been thoroughly investigated both experimentally as well as computationally. We have previously shown that, without proper treatment of dispersion, one can not adequately predict important structural features or dynamic properties, for example, bowl depth, barrier, and kinetic isotope effects.[1] Further investigations revealed that vdW attractive forces among the peripheral *endo*-methyl groups in this case could contribute to a stabilization of the bowl (ground state) relative to the flat form (transition state), thereby increasing the barrier height. The structure represented a computational challenge not only for DFT methods but also for conventional methods because of its large size.

Geometry optimizations carried out using several functionals are reported in Table 7. While B3LYP/cc-pVDZ quite accurately predicts basic structural parameters, as well as bowl depth and curvature, for essentially all previously investigated corannulene derivatives, the functional comes short for *sym*-pentamanisylcorannulene. Of the bond lengths, the edge bonds (leyward flank and rim bonds) have the largest error compared to experiment, both overestimated by 1 ppm. M06−2X does much better but is still is off by nearly 1 ppm for the C−C hub bond.

The prediction of bowl depth and associated methyl/methyl distances and torsions are more challenging. B3LYP/cc-pVDZ would predict a bowl depth of 0.85 Å, compared to the experimental value of 0.91 Å. Given a structure−correlation formula of $E = ax^4 - bx^2$, this difference in bowl depth would translate into a large underestimation of the barrier to inversion, as is verified in the computation at 8.84 kcal/mol. Correction with the MP2 single point then overshoots

Table 7. Computed Geometry of *sym*-1,3,5,7,9-Pentamanisylcorannulene Compared to Experimental Geometry for a Variety of Density Functionals

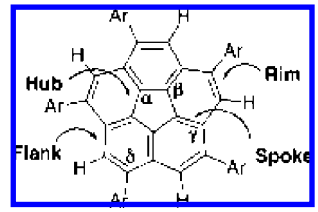

parameter	B3LYP	M06−2X	B97D	B97D opt	revPBE opt	MP2	exptl
C−C hub (Å)	1.418	1.420	1.4264	1.4252	1.4539	1.4245	1.413(4)
C−C spoke (Å)	1.385	1.381	1.3989	1.3975	1.4233	1.4051	1.382(4)
C−C flank (Å)	1.461	1.455	1.4580	1.4601	1.4908	1.4527	1.452(4) leyward
	1.450	1.446	1.4476	1.4496	1.4802	1.4442	1.446(4) wayward
C−C rim (Å)	1.399	1.388	1.4016	1.4033	1.4279	1.4099	1.381(8)
angle α (sym) (deg)	108.0	108.0	108.0	108.0	108.0	108.0	108.0(4)
angle β (sym) (deg)	123.4	122.8	122.5	122.0	122.0	122.4	124.3(4)
angle γ (sym) (deg)	114.8	115.4	115.9	115.6	115.7	115.8	111.9(4)
angle δ (sym) (deg)	120.3	120.6	120.3	120.4	120.3	120.7	122.2(4)
bowl depth (Å)	0.85	0.94	1.02	0.98	1.01	1.01	0.91
$Me_{endo}(1)-Me_{endo}(2)$ (Å)	4.62	4.35	4.24	4.37	4.4	4.2	4.4
$Me_{endo}(1)-Me_{endo}(3)$ (Å)	7.47	7.04	6.86	7.08	7.14	6.76	7.1
Ar−Cor torsion (deg)	79.6	72.2	82.4	83.7	83.4		79
inversion barrier (kcal/mol)	8.84(14.09) [a]	12.65	16.6	14.2	14.2		12.2−12.5

[a] MP2/cc-pVDZ//B3LYP/cc-pVDZ.

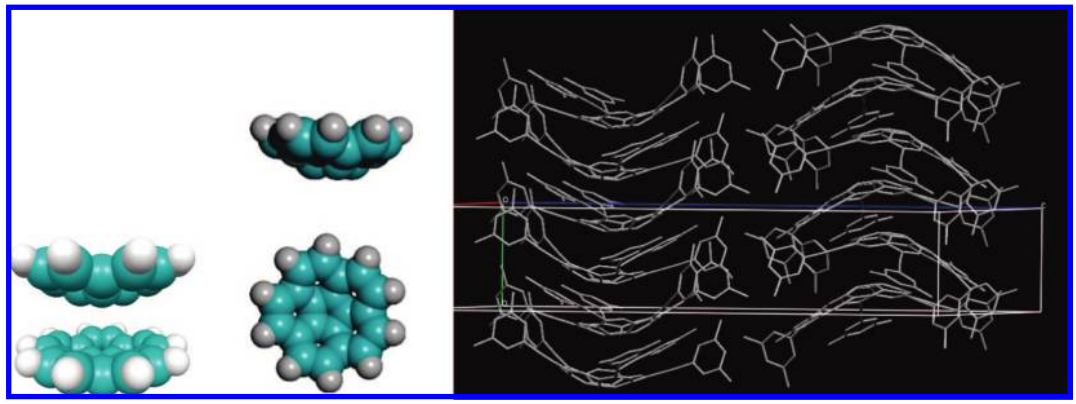

Figure 22. Example of stacking motifs and packing of corannulene and functionalized corannulene.

the barrier by a significant amount at 14.09 kcal/mol, but this can be expected because the depth of the bowl is not correct, and only the dispersion effects at the B3LYP/cc-pVDZ predicted geometry are included. M06−2X predicts the bowl depth to be slightly deeper (0.03 Å) than experimental predictions, and thus the barrier to inversion is also about 1 kcal/mol too high. In all of the semiempircally corrected functionals, B97D, B97D with optimized s_6, and revPBE with optimized s_6, the geometry of the base corannulene nucleus is not as good as with our standard, B3LYP, predicting bonds that are longer than experiment in most cases, although B97D is quite good. The revPBE with optimized s_6 parameters is quite far off in the bond lengths of the basic corannulene nucleus, and overestimates the bowl depth. In terms of bowl depth and barrier prediction, the B97D with optimized s_6 parameter is slightly better than MP2/cc-pVDZ, at a significant reduction in computational cost.

Higher-Order Constructs of Corannulene. The ability to model intercorannulene interactions, as associated with packing in the crystal or complexes of substituted stacked corannulenes, is very much associated with proper modeling of vdW interactions, (Figure 22). For example, interesting packing characteristics have been observed in the experimental crystal structures depending on functionalization, resulting in important materials properties.[4,102−106] Even though corannulene itself is not a $4n + 2$ Hückel system, the electronic structure would suggest a configuration that allows for a 6-electron cyclopentadienyl anion in the center, and a 14-electron cation as the outermost ring, each of which does satisfy a $4n + 2$ cycle ($n = 2$ and $n = 3$, respectively). In addition, experimentally, corannulene behaves like other aromatic compounds, for example undergoing electrophilic substitution reactions. As such, one might expect stability for dimers, trimers, and higher-order stacks, dominated by vdW interactions. We are therefore in the process of considering larger corannulene dimers and stacks with the new dispersion models. As an example, the dimer computation on the PS conformation of corannulene, with B3LYP/cc-pVDZ and B97D/cc-pVDZ, predict interstack distances

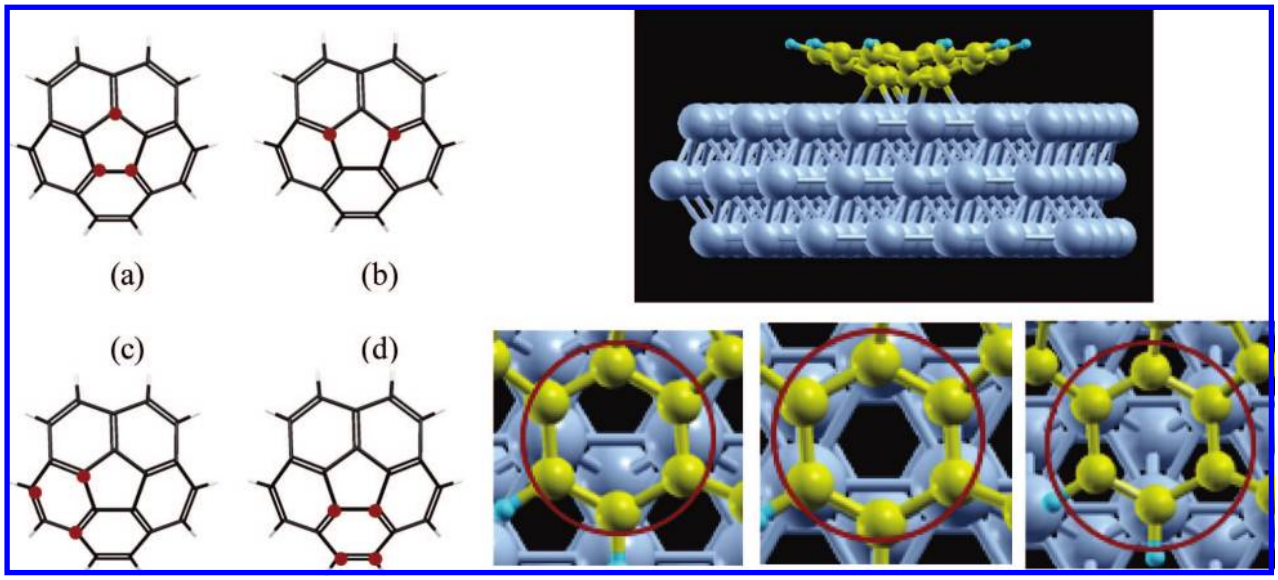

Figure 23. (Left) Possible binding motifs of corannulene on Cu(111): (a) η^5-hollow site, (b) η^5-bridge site, (c) η^6-hollow site, (d) η^6-bridge site. (Right, top) One conformation of corannulene on Cu(111) surface. (Right, bottom) hcp hollow site, bridge site, and fcc-hollow site.

of 4.63 and 3.55 Å, respectively. Because of the much larger surface area of corannulene over benzene, we see a much larger effect of dispersion, further illustrating the inadequacy of B3LYP. In addition, only for the B97D is the stack predicted to be bound, by 6.23 kcal/mol, significantly more than found for the benzene dimer. Further investigations of stacks and functionalized stacks are now ongoing.

Alternatively, it is of interest to investigate binding characteristics of metal−organic complexes composed of (substituted) corannulenes with a planar metal surface. [107,108] Such studies enable investigation of molecular self-organization processes of adsorbate molecules on the surface that can be responsible for formation of supramolecular aggregates. Two-dimensional assembly into supramolecular structures is of great interest for study of fundamental processes, such as molecular [109,110] and chiral recognition. [111−116] Moreover, functionalization of surfaces by adsorption of large organic molecules appears to be an important route toward new materials or templates for heterogeneous catalysis [117] and molecular electronics. [118]

Attempts to incorporate solutions to failures involving nonlocal, long-range electron correlation directly into a density functional can result in rather complicated formulations, leading to expressions at least as complex as some wave function methods. Examples include the vdW-DFT method that has just recently been implemented in the SIESTA software [54,55] and the first principles approach suggested by Kohn, [119] which breaks the Coulomb interaction into a short and long-range (adiabatic connection formula) component of which only the long-range contributes to the vdW energies. Ongoing work with the SIESTA group involves further testing the vdW-DFT method in the SIESTA software and considerations of practicality for the ongoing corannulene on surface computations.

Motivated by the work involving the semiempircally corrected DFT fucntionals, we have in the meantime proceeded to implement a protocol for investigations involving complex Cu(111) + corannulene surface interactions, using GAMESS, together with the surface modeling software, SIESTA, the latter of which also now has the semiempirical dispersion correction implemented. We have tested this method out on various conformational possibilities of corannulene on a 3 layer Cu(111) surface, as depicted in Figure 23.

Table 8. Computed Geometry of Corannulene Conformations on Cu(111) Surface, Comparing the revPBE Functional with and without Empirical Dispersion Correction

parameter[a]	revPBE	revPBE-D
η^6-bridge fcc site	2.46 Å	2.23 Å
η^6-hollow fcc site	2.37 Å	2.16 Å
η^6-hollow hcp site	2.38 Å	2.18 Å
η^5-bridge site	detaches	
η^5-hollow hcp site	2.5 Å	2.36 Å

[a] Average C−C bond length for ring.

While results suggest that functionals, such as B3LYP, revPBE, or BLYP, all predict the corannulene + Cu(111) to be repulsive or only weakly bound, depending on the particular conformation of corannulene on the surface, the semiempirical correction enables more realistic modeling of the complexation process (Table 8). Using a double-ζ quality basis set supplemented with extra diffuse functions for the copper surface, we are able to perform computation of corannulene in several different conformational possibilities on a 3-layer slab of Cu(111) plus corannulene. These preliminary results show promise for realistic modeling on a metallic surface, as compared to known STM results on the same system, enabling a more detailed research investigation including an increase to a 6-layer slab, which will be the subject of a future publication.

Conclusions

At the onset of this work, our major concerns were to implement more optimal DFT functionals for the purpose

Table 9. Summary of Density Functional Plus s_R/s_6 Coefficient Combinations Proposed for a Variety of Basis Sets, As Determined from Predictions of S22 Complexes

DFT functional	basis set	s_R value	optimized s_6 value	MAD (kcal/mol)
B97D	cc-pVDZ	1.1	1.00	1.075
	cc-pVDZ+CP	1.1	1.39	0.518
	cc-pVTZ	1.1	1.18	0.337
	cc-pVTZ+CP	1.1	1.41	0.454
	cc-pVQZ	1.1	1.26	0.330
	cc-pVQZ+CP	1.1	1.39	0.441
	TZV(2d,2p)	1.1	1.25	0.375
	TZV(2d,2p)+CP	1.1	1.38	0.425
B3LYP	cc-pVDZ	1.1	0.73	1.709
	cc-pVTZ	1.1	0.88	0.853
	cc-pVQZ	1.1	0.96	0.612
PBE	cc-pVDZ	1.1	0.50	2.579
	cc-pVTZ	1.1	0.64	1.030
	cc-pVQZ	1.1	0.65	0.798
revPBE	cc-pVDZ	1.1	1.66	0.826
	cc-pVTZ	1.1	1.87	1.326
	cc-pVQZ	1.1	1.90	1.536
	cc-pVTZ (8−22)	1.1	1.87	0.393
	cc-pVQZ (8−22)	1.1	1.90	0.355
B2PLYP	cc-pVDZ	1.3	1.55	1.394
	cc-pVTZ	1.3	1.55	0.517

of accurate predictions of large molecular polynuclear carbon-based complexes and corannulene on copper surfaces, all of which have dominant dispersion interactions. We have implemented several additional functionals into GAMESS, together with a semiempirical dispersion correction that can be applied with these and other functionals within GAMESS. We have also implemented and tested the B2PLYP double-hybrid functional. For functionals with a semiempircal correction, we have carried out a double parameter optimization to understand the variation in the s_R and s_6 coefficients with respect to basis set, functional type, and BSSE, and have proposed optimal values, a summary of which is shown in Table 9. We find overall good performance in particular of the B97D functional. In addition, we find a convenient convergence of optimal s_6 parameter of 1.4 when BSSE is considered for the S22 set of molecules using any of the series cc-pVnZ, $n = 2-4$, as well as TZV2P, a suggested value to use when CP corrections are applied with B97D, even though it is a relatively large value compared to non-CP-corrected values. The global performance of B97D+CP in terms of MAD of the S22 set shows a slight loss of accuracy within the same basis sets, which is attributed to the error associated with the CP corrections, providing a reasonable estimate of the error associated with CP within the S22 set of molecules. Future studies will look at this phenomenon more globally.

Comparative results across functionals were given for several applications with high degree of dispersive interactions, illustrating the strengths and weaknesses in these functionals. Consistently reliable results are found for several of the functional strategies, including the exchange-correlation functional provided by BMK, the M06−2X functional, and the semiempirically corrected B97D functional. The double hybrid functional, B2PLYP functional is also seen to provide very good performance, but with an associated higher cost for the MP2 evaluation.

A second purpose of this work was to create a reliable protocol for investigations of polynuclear aromatic carbon species, such as corannulene, on metallic surface. Our investigations here were initially limited to the PBE and revised-PBE functionals in the SIESTA software, a linear-scaling density functional package designed for studies involving materials. Including the semiempirical dispersion correction was seen to greatly enhance predictability of the functionals, as demonstrated in the GAMESS/SIESTA hybrid method for corannulene on Cu(111) surface results, particularly considering other strategies are too costly. Our initial investigations are quite promising, and with the results obtained in our investigations shown here, we are now actively pursuing these new capabilities with a larger Cu(111) surface.

Acknowledgment. This work was supported by the Swiss National Science Foundation. S. Grimme and D. Truhlar are both acknowledged for their helpful discussions and insights. L. Zoppi, a postdoctoral associate in the Baldridge group, is acknowledged for her work involving corannulene on copper surface with GAMESS and SIESTA.

References

(1) Hayama, T.; Baldridge, K. K.; Wu, Y.-T.; Linden, A.; Siegel, J. S. *J. Am. Chem. Soc.* **2008**, *130*, 1583.

(2) Petrukhina, M. A. *Angew. Chem., Int. Ed. Engl.* **2008**, *47*, 1550.

(3) Tiwary, A. S.; Mukherjee, A. K. *THEOCHEM* **2008**, *859*, 107.

(4) Wu, Y. T.; Bandera, D.; Maag, R.; Linden, A.; Baldridge, K. K.; Siegel, J. S. *J. Am. Chem. Soc.* **2008**, *120*, 1.

(5) Betowski, L. D.; Enlow, M.; Riddick, L.; Aue, D. H. **2007**, *111*, 3672.

(6) Mack, J.; Vogel, P.; Jones, D.; Kaval, N.; Sutton, A. *Org. Biomol. Chem.* **2007**, *5*, 2448.

(7) Hayama, T.; Wu, Y.-T.; Linden, A. L.; Baldridge, K. K.; Siegel, J. S. *J. Am. Chem. Soc.* **2007**, *129*, 12612.

(8) Yamaji, M.; Teakehira, K.; Mikoshiba, T.; Sachiko, T.; Okada, Y.; Fujitsuka, M.; Majima, T.; Tobita, S.; Nishimura, J. *Chem. Phys. Lett.* **2006**, *425*, 53.

(9) Seiders, T. J.; Baldridge, K. K.; Grube, G. H.; Siegel, J. S. *J. Am. Chem. Soc.* **2001**, *123*, 517.

(10) Seiders, T. J.; Baldridge, K. K.; Siegel, J. S. *J. Am. Chem. Soc.* **1999**, *121*, 7439.

(11) Kutzelnigg, W. Pair correlation theories.In *Modern Theoretical Chemistry*; Schaefer, H. F. ,Ed.; Plenum Press: New York, 1977; pp 129.

(12) Kutzelnigg, W. *Einführung in der Theoretische Chemie*; Verlag Chemie *:* Weinheim, Germany, 1978; Vol. 2

(13) Helgaker, T. ; Jørgensen, P.; Olsen, J. *Molecular Electronic-Structure Theory*; J. Wiley: New York, 2000.

(14) Møller, C.; Plesset, M. S. *Phys. Rev.* **1934**, *46*, 618.

(15) Bates, D. M.; erson, J. A.; Oloyede, P.; Tschumper, G. S. *Phys. Chem. Chem. Phys.* **2008**, *10*, 2775.

(16) Bachorz, R. A.; Bischoff, F. A.; Hoefener, S.; Klopper, W.; Ottiger, P.; Leist, R.; Frey, J. A.; Leutwyler, S. *Phys. Chem. Chem. Phys.* **2008**, *10*, 2758.

(17) Meyer, E. A.; Castellano, R. K.; Diederich, F. *Angew. Chem., Int. Ed.* **2003**, *42*, 1210.

(18) Nishio, M. *CrystEngComm* **2004**, *6*, 130.

(19) Bauschlicher, C. W. , Jr.; Ricca, A.; Partridge, H.; Langhoff, S. R. Chemistry by density functional theory. In *Recent Advances in Density Functional Methods, Part II*; Chang, D. P. , Ed.; World Scientific: Singapore, 1997.

(20) Martin, J. M. L. Some observations and case studies on basis set convergence in density functional theory. In *Density Functional Theory: A Bridge between Chemistry and Physics*; Geerlings, P., De Proft, F., Langenaeker, W. , Eds.; VUB Press: Brussels, Belgium, 2000.

(21) Boese, A. D.; Martin, J. M. L. *J. Chem. Phys.* **2004**, *121*, 3405.

(22) Zhao, Y.; Schultz, N. E.; Truhlar, D. G. *J. Chem. Phys.* **2005**, *123*, 161103/1.

(23) Zhao, Y.; Truhlar, D. G. *Theor. Chem. Acc.* **2008**, *120*, 215.

(24) Grimme, S. *J. Comput. Chem.* **2006**, *27*, 1787.

(25) Grimme, S. *J. Chem. Phys.* **2006**, *124*, 034108.

(26) Zhao, Y.; Truhlar, D. G. *Acc. Chem. Res.* **2008**, *41*, 157.

(27) Benighaus, T.; DiStasio, R. A.; Lochan, R. C.; Chai, J.-D.; Head-Gordon, M. *J. Phys. Chem. A.* **2008**, *112*, 27002.

(28) Hill, J. G.; Platts, J. A.; Werner, H.-J. *Phys. Chem. Chem. Phys.* **2008**, *8*, 4072.

(29) Silvestrelli, P. L. *Phys. Rev. Lett.* **2008**, *100*, 053002.

(30) Tarnopolsky, A.; Karton, A.; Sertchook, R.; Vuzman, D.; Martin, J. M. L. *Phys. Chem. A* **2008**, *112*, 3.

(31) Riley, K. E.; Vondrasek, J.; Hobza, P. *Phys. Chem. Chem. Phys.* **2007**, *9*, 5555.

(32) Schwabe, T.; Grimme, S. *Phys. Chem. Chem. Phys.* **2007**, *9*, 3397.

(33) Grimme, S.; Antony, J.; Schwabe, T.; Mück-Lichtenfeld, C. *Org. Biomol. Chem.* **2007**, *5*, 741.

(34) Grimme, S.; Mück-Lichtenfeld, C.; Antony, J. *J. Phys. Chem. C* **2007**, *111*, 11199.

(35) Neese, F.; Schwabe, T.; Grimme, S. *J. Chem. Phys.* **2007**, *126*, 124115.

(36) Grimme, S.; Neese, F. *J. Chem. Phys.* **2007**, *127*, 154116.

(37) Grimme, S.; Steinmetz, M.; Korth, M. *J. Chem. Theor. Comput.* **2007**, *3*, 42.

(38) Zhao, Y.; Truhlar, D. G. *J. Chem. Theor. Comput.* **2006**, *2*, 1009.

(39) Jurecka, P.; Cerny, J.; Hobza, P.; Salahub, D. R. *J. Comput. Chem.* **2006**, *28*, 555.

(40) Grimme, S. *J. Comput. Chem.* **2004**, *25*, 1463.

(41) Lilienfeld, O. A.; Tavernelli, L.; Rothlisberger, U. *Phys. Rev. Lett.* **2004**, *93*, 153004.

(42) Wu, Q.; Yang, W. *J. Chem. Phys.* **2002**, *116*, 515.

(43) Wu, X.; Vargas, M. C.; Nayak, S.; Lotrich, V.; Scoles, G. *J. Chem. Phys.* **2001**, *116*, 8748.

(44) Mooij, W. T. M.; van Duijneveldt, F. B.; van Duijneveldt-van de Rijdt, J. G.C.M.; van Eijck, B. P *J. Phys. Chem. A.* **1999**, *103*, 9872.

(45) Becke, A. D. *J. Chem. Phys.* **1997**, *107*, 8554.

(46) Meijer, E. J.; Sprik, M. *J. Chem. Phys.* **1996**, *105*, 8684.

(47) Perdew, J. P.; Burke, K.; Ernzerhof, M. *Phys. Rev. Lett.* **1996**, *77*, 3865.

(48) Hobza, P.; Zahradnik, R. *Chem. Rev.* **1988**, *88*, 871.

(49) Kristyan, S.; Pulay, P. *Chem. Phys. Lett.* **1994**, *229*, 175.

(50) Hobza, P.; Sponer, J.; Reschel, T. *J. Comput. Chem.* **1995**, *16*, 1315.

(51) Pérez-Jordá, J. M.; Becke, A. D. *Chem. Phys. Lett.* **1995**, *233*, 134.

(52) Schmidt, M.; Baldridge, K. K.; Boatz, J. A.; Elbert, S.; Gordon, M.; Jenson, J. H.; Koeski, S.; Matsunaga, N.; Nguyen, K. A.; Su, S. J.; Windus, T. L.; Dupuis M.; Montgomery, J. A. *J. Comput. Chem.* **1993**, *14,* 1347.

(53) Soler, J. M.; Artacho, E.; Gale, J. D.; Garcia, A.; Junquera, J.; Ordejón, P.; Sánchez-Portal, D. *J. Phys.: Condens. Matter* **2002**, *14*, 2745.

(54) Dion, M.; Rydberg, H.; Schroeder, E.; Langreth, D. C.; Lundqvist, B. I. *Phys. Rev. Lett.* **2004**, *92*, 246.

(55) Langreth, D. C.; Dion, M.; Rydberg, H.; Schroeder, E.; Hyldgaard, P.; Lundqvist, B. I *Int. J. Quantum Chem.* **2004**, *101*, 599.

(56) Zhang, Y.; Yang, W. *Phys. Rev. Lett.* **1998**, *80*, 890.

(57) Becke, A. D. *Phys. Rev. A* **1988**, *38*, 3098.

(58) Perdew, J. P. *Phys. Rev. B.* **1986**, *33*, 8822.

(59) Perdew, J. P. *Phys. Rev. B.* **1986**, *23*, 7046.

(60) Becke, A. D. *J. Chem. Phys.* **1993**, *98*, 5648.

(61) Lee, C.; Yang, W.; Parr, R. G. *Phys. Rev. B.* **1988**, *37*, 785.

(62) Schäfer, A.; Huber, C.; Ahlrichs, R. *J. Chem. Phys.* **1994**, *100*, 5829.

(63) Dunning, T. H. *J. Chem. Phys.* **1989**, *90*, 1007.

(64) Jurecka, P.; Sponer, J.; Cerny, J.; Hobza, P. *Phys. Chem. Chem. Phys.* **2006**, *8*, 1985.

(65) Zimmerli, U.; Parrinello, M.; Koumotsakos, P. *J. Chem. Phys.* **2004**, *120*, 2693.

(66) Kubar, T.; Jurecka, P.; Cerny, J.; Rezáe, J.; Otyepka, M.; Valdés, H.; Hobza, P. *J. Phys. Chem. A* **2007**, *111*, 5642.

(67) Ahlrichs, R.; Penco, R.; Scoles, G. *Chem. Phys.* **1977**, *19*, 119.

(68) Hepburn, J.; Scoles, G. *Chem. Phys. Lett.* **1975**, *36*, 451.

(69) Zhang, Y.; Yang, W. *Phys. Rev. Lett.* **1997**, *80*, 890.

(70) Williams, R.; Malhotra, D. *Chem. Phys.* **2006**, *327*, 54.

(71) Ducere, J.-M.; Cavallo, L *J. Phys. Chem. B.* **2007**, *111*, 13124.

(72) Perdew, J. P.; Schmidt, K. Density functional theory and its application to materials. Presented at the AIP Conference, 2000, Antwerp, Belgium.

(73) Zhao, Y.; Lynch, B. J.; Truhlar, D. G *J. Phys. Chem. A.* **2004**, *108*, 4786.

(74) Zhao, Y.; Lynch, B. J.; Truhlar, D. G. *Phys. Chem. Chem. Phys.* **2005**, *7*, 43.

(75) GAMES M06 series of functionals implemented by Sarom Sok, Ames, Iowa, unpublished work.

(76) Schamp, J., H.W.; Mason, E. A.; Richardson, A. C. B.; Altman, A *Phys. Fluids* **1958**, *1*, 329.

(77) Dymond, J. H.; Rigby, M.; Smith, E. B. *J. Chem. Phys.* **1965**, *42*, 2801.

(78) Snook, I. K.; Spurling, T. H. *J. Chem. Soc., Faraday Trans. 2* **1972**, *68*, 1359.

(79) Hanley, H. J. M.; Klein, M. *J. Phys. Chem.* **1972**, *76*, 1743.

(80) Pope, G. A.; Chappelear, P. S.; Kobayashi, R. *J. Chem. Phys.* **1973**, *59*, 423.

(81) Matthews, G. P.; Smith, E. B. *Mol. Phys.* **1976**, *32*, 1719.

(82) Janseb, H. B.; Ross, P. *Chem. Phys. Lett.* **1969**, *3*, 140.

(83) Boys, S. F.; Bernardi, F. *Mol. Phys.* **1970**, *19*, 553.

(84) Dunning, T. H. *J. Chem. Phys.* **1971**, *55*, 716.

(85) Sinnokrot, M. O.; Sherrill, C. D. *J. Phys. Chem. A.* **2004**, *108*, 10200.

(86) Grover, J. R.; Walters, E. A.; Hui, E. T. *J. Phys. Chem.* **1987**, *91*, 3233.

(87) Lee, E. C.; Kim, D.; Jurecka, P.; Tarakeshwar, P.; Hobza, P.; Kim, K. S. *J. Phys. Chem. A* **2007**, *111*, 3446.

(88) Ringer, A. L.; Sinnokrot, M. O.; Lively, R. P.; Sherrill, C. D. *Chem.—Eur. J.* **2006**, *12*, 3821.

(89) Sinnokrot, M. O.; Sherrill, C. D. *J. Phys. Chem. A* **2006**, *110*, 10656.

(90) Sinnokrot, M. O.; Sherrill, C. D. *J. Am. Chem. Soc.* **2004**, *126*, 7690.

(91) Sinnokrot, M. O.; Sherrill, C. D. *J. Phys. Chem. A.* **2003**, *107*, 8377.

(92) Cozzi, F.; Cinquini, M.; Annunziata, R.; Dwyer, T.; Siegel, J. S. *J. Am. Chem. Soc.* **1992**, *114*, 5729.

(93) Cozzi, F.; Cinquini, M.; Annuziata, R.; Siegel, J. S. *J. Am. Chem. Soc.* **1993**, *115*, 5330.

(94) Cozzi, F.; Ponzini, F.; Annunziata, R.; Cinquini, M.; Siegel, J. S. *Angew. Chem., Int. Ed. Engl.* **1995**, *34*, 1019.

(95) Cozzi, F.; Siegel, J. S. *Pure Appl. Chem.* **1995**, *67*, 683.

(96) Zoltewicz, J. A.; Maier, N. A.; Fablan, W. M. F. *J. Org. Chem.* **1998**, *63*, 4985.

(97) Kaneta, N.; Mitamura, F.; Uemura, M.; Murata, Y.; Komatsu, K. *Tetrahedron* **1996**, *37*, 5835.

(98) Cozzi, F.; Annunziata, R.; Benaglia, M.; Cinquini, M.; Raimondi, L.; Baldridge, K. K.; Siegel, J. S. *J. Org. Biomol. Chem.* **2002**, *1*, 1.

(99) Cozzi, F.; Annunziata, R.; Benaglia, M.; Baldridge, K. K.; Aguirre, G.; Sritana-Anat, Y.; Siegel, J. S. *Phys. Chem. Chem. Phys.* **2008**, *10*, 2686.

(100) Lovas, F. J.; McMahon, R. J.; Grabow, J.-U.; Schnell, M.; Mack, J.; Scott, L. T.; Kuczkowski, R. L. *J. Am. Chem. Soc.* **2004**, *127*, 4345.

(101) Seiders, T. J.; Baldridge, K. K.; Gleiter, R.; Siegel, J. S. *Tetrahedron Lett.* **2000**, *41*, 4519.

(102) Zhao, M.; Truhlar, D. G. *Phys. Chem. Chem. Phys.* **2008**, *10*, 2813.

(103) Filatov, A. S.; Petrukhina, M. A. *J. Organomet. Chem.* **2008**, *693*, 1590.

(104) Wu, Y.-T.; Siegel, J. S. *Chem. Rev.* **2006**, *106*, 4843.

(105) Prinzbach, H.; Wahl, F.; Weiler, A.; Landenberger, P.; Woerth, J.; Scott, L. T.; Gelmont, M.; Olevano, D.; Sommer, F.; von Issendorff, B. *Chem.—Eur. J.* **2006**, *12*, 6268.

(106) Diudea, M. V. *Phys. Chem. Chem. Phys.* **2005**, *7*, 3626.

(107) Parschau, M.; Fasel, R.; Ernst, K.-H.; Groening, O.; Brandenberger, L.; Schillinger, R.; Greber, T.; Seitsonen, A. P.; Wu, Y.-T.; Siegel, J. S. *Angew. Chem., Int. Ed.* **2007**, *46*, 8258.

(108) Xiao, W.; Passerone, D.; Ruffieux, P.; Aiet-Mansour, K.; Groening, O.; Tosatti, E.; Siegel, J. S.; Fasel, R. *J. Am. Chem. Soc.* **2008**, *130*, 4767.

(109) Theobald, J. A.; Oxtoby, N. L.; Phillips, M. A.; Champness, N. R.; Beton, P. H. *Nature* **2003**, *424*, 1029.

(110) Yokoyama, T.; Yokoyama, S.; Kamikado, T.; Okuno, Y.; Mashiko, S. *Nature* **2001**, *413*, 619.

(111) Fasal, R.; Parschau, M.; Ernst, K.-H. *Angew. Chem., Int. Ed.* **2003**, *43*, 2853.

(112) Parschau, M.; romer, S.; Ernst, K.-H. *J. Am. Chem. Soc.* **2004**, *126*, 15398.

(113) Chen, Q.; richardson, N. V. *Nat. Mater.* **2003**, *2*, 324.

(114) Fasel, R.; Parschau, M.; Ernst, K.-H. *Angew. Chem., Int. Ed.* **2003**, *42*, 5177.

(115) Greber, T.; Sljivancanin, Z.; Schillinger, R.; Wider, J.; Hammer, B. *Phys. Rev. Lett.* **2006**, *96*, 056103.

(116) Schillinger, R.; Sljivancanin, Z.; Hammer, B.; Greber, T. *Phys. Rev. Lett.* **2007**, *98*, 136102.

(117) Wan, T. A.; Davies, M. E. *Nature* **1994**, *370*, 449.

(118) Ratner, M. *Nature* **2005**, *435*, 575.

(119) Kohn, W.; Meir, Y.; Makarov, D. E. *Phys. Rev. Lett.* **1998**, *80*, 4153.

CT800252Z